



HAL
open science

Multi-Directional Continuous Traffic Model For Large-Scale Urban Networks

Liudmila Tumash, Carlos Canudas de Wit, Maria Laura Delle Monache

► **To cite this version:**

Liudmila Tumash, Carlos Canudas de Wit, Maria Laura Delle Monache. Multi-Directional Continuous Traffic Model For Large-Scale Urban Networks. 2021. hal-03236552v1

HAL Id: hal-03236552

<https://hal.science/hal-03236552v1>

Preprint submitted on 26 May 2021 (v1), last revised 5 Dec 2021 (v2)

HAL is a multi-disciplinary open access archive for the deposit and dissemination of scientific research documents, whether they are published or not. The documents may come from teaching and research institutions in France or abroad, or from public or private research centers.

L'archive ouverte pluridisciplinaire **HAL**, est destinée au dépôt et à la diffusion de documents scientifiques de niveau recherche, publiés ou non, émanant des établissements d'enseignement et de recherche français ou étrangers, des laboratoires publics ou privés.

Multi-Directional Continuous Traffic Model For Large-Scale Urban Networks

Liudmila Tumash^a, Carlos Canudas-de-Wit^a, Maria Laura Delle Monache^{b,*}

^a*Univ. Grenoble Alpes, CNRS, Inria, Grenoble INP, GIPSA-Lab*

^b*Univ. Grenoble Alpes, Inria, CNRS, Grenoble INP, GIPSA-Lab*

Abstract

In this paper we propose a new multi-direction traffic flow model called the NSWE-model. This macroscopic model is composed by a set of four partial differential equations (PDEs), each modelling the density propagation in one of the four cardinal directions: North, South, West and East. We show step-by-step the formal derivation of this continuous model from the classical cell transmission model at intersections. We use only the knowledge about the network topology (location of the roads) and network infrastructure parameters such as roads maximal speeds, number of lanes and capacities. The information about the flow direction is retrieved from the turning ratios at the intersections, which is then aggregated in four directions using projection matrices. Additionally, we discuss the mathematical properties of the NSWE-model. In particular, we show that this model is hyperbolic and corresponds to a conservation law, where the conserved quantity is the total vehicle density in the network. The model is validated using synthetic data from the microsimulator Aimsun that takes Grenoble downtown as a network input. Moreover, the model is also validated using real data collected from real sensors installed in Grenoble.

Keywords: Macroscopic traffic flow model, partial differential equations, simulation and validation, continuation of ODE to PDE, large-scale urban

*Corresponding author

Email addresses: liudmila.tumash@gipsa-lab.fr (Liudmila Tumash),
carlos.canudas-de-wit@gipsa-lab.grenoble-inp.fr (Carlos Canudas-de-Wit),
ml.dellemonache@inria.fr (Maria Laura Delle Monache)

1. Introduction

On the level of traffic management it is essential to be able predict how traffic conditions could evolve within several hours. This makes traffic modelling an important issue to study due to ever-growing demand for transportation in urban areas. Yearly people spend hundreds of hours in traffic jams, which requires development of novel techniques allowing to predict traffic propagation and transportation management solutions.

The development of traffic flow models, based on the conservation of vehicles, has been mostly influenced by the Lighthill-Whitham-Richards model (LWR) proposed in the fifties by [1] and [2]. This model describes the propagation of traffic flow as if it was a compressible fluid. It is also assumed there exists a relation between average flow and average density along the road called Fundamental Diagram (FD). Later on, a time-discrete approximation of the LWR was introduced by [3], which is now known as the cell transmission model (CTM). The CTM-model is based on the demand-supply concept, and it is now the most popular model in the traffic community due to its simplicity.

In its original formulation the LWR-model is applicable only to single roads of infinite length. Extension to networks required developing a methodology for intersection modelling within the LWR-framework, which was first done at the end of last century by [4] who considered a network of unirectional roads. Later on, this formulation was refined to capture multidirectional traffic, e.g. see [5]. The CTM model has also been extended to networks in [6], who considered networks as directed graphs consisting of links (roads) and nodes (junctions). The general theory of traffic flow on networks is presented in [7]. However, traffic modelling might become tedious on large networks containing thousands of roads due to a high computational cost which is determined by the number of roads and junctions in a network.

For urban traffic modelling, one can also use continuous macroscopic models

that describe traffic as a two-dimensional fluid moving on a continuum plane that corresponds to a dense urban network. This approach has various advantages, e.g., the problem size does not depend on the number of roads as well as less data are required for the model setup. Early works on continuous traffic models appeared several decades ago [8, 9, 10], and their focus was to determine equilibrium in urban networks. However, due to the lack of any knowledge on a flow-density relation on a city level, these static models could not predict traffic dynamics in rush hours (see [11] for a general review).

A relation between average density and average flow on a city level known as Macroscopic Fundamental Diagram (MFD) has been empirically established from the data collected in Yokohama, Japan [12, 13]. This discovery triggered development of multi-reservoir models that correspond to ordinary differential equations describing the change in the number of cars in some zone (reservoir) per time unit. Thereby, the information about inflows and outflows of a reservoir is obtained from MFD. Having only few parameters to tune and a low computational cost, MFD-based models are now widely used. The main drawback of this approach arises when a zone consists of links whose congestion level has a large variance. This problem could be overcome using partitioning algorithms that divide an area such that each zone has a well-defined MFD [14, 15]. However, in case of rapidly changing traffic conditions (e.g., accident on a road), the MFD-based approach may be inefficient, since it requires applying partitioning algorithms every time the congested region moves, see [16] for more details.

Another way to describe the evolution of traffic in cities is to use dynamic two-dimensional continuum models, see [17] for a review. These models share a lot of features with pedestrian models [18] with the difference that the direction of the traffic flow propagation is restricted to the underlying urban network topology. Some of the traffic models [19, 20] are based on solving Eikonal equations to determine the direction of the lowest cost of the flow propagation. A recent work [21] introduced a two-dimensional LWR model that uses the network topology to determine the direction of the traffic flow by including space-dependence into the fundamental diagram.

Most of the studies on two-dimensional traffic evolution consider models having a unique direction of motion, while only few of them consider anisotropic conditions, i.e., multi-directional traffic. The first work considering multiple directions of flow appeared quite recently [22]. This work took inspiration from pedestrian modelling by considering a poly-centric urban city as a continuum, in which the path is chosen according to the dynamic user-optimal principle. However, this model has several drawbacks such as the density that might violate its maximal possible value. There exist other works [23, 24] proposing two-dimensional multi-layer models. In both of these works each layer is coupled to other layers but mixing between them is not included, i.e., vehicles can not change their layers. In [23] the model design is based on network topology, while in [24] the model is based on MFD. Furthermore, both of these models can sometimes lose hyperbolicity.

To cope with some of these limitations, in this paper, we propose a new multi-directional two-dimensional continuous traffic NSWE-model. It consists of four partial differential equations (PDEs) that describe the evolution of the vehicle density in four cardinal directions: North, South, West and East. We use the information on network topology, turning ratios at each intersection and infrastructure parameters.

Our main contribution is the formal derivation of the macroscopic model describing traffic propagation in some large traffic network by using the classical CTM-model at each intersection. The resulting NSWE-model is a hyperbolic system with bounded densities in each layer, and the model corresponds to a conservation law. The main novelty of our model is that it includes mixing between different density layers, i.e., it allows cars to change their original direction of movement. For example, imagine a car going to the North that changed its direction and went to the East, thus there is a non-zero flow from North to East layer. We present a method allowing to transform traffic evolving on arbitrarily sparse networks into a continuum model, which is a beneficial form when it comes to modelling on a large scale.

The structure of this paper is the following. In Section 2, we review the CTM

model for one intersection, thereby introducing several important assumptions. In Section 3, we present the NSWE-framework used to derive the NSWE-model from the CTM-model in Section 4, where the model is expanded to cover the whole network by the continuation method presented in [25] that turns an ordinary differential equation into a partial differential equation. In Section 5, the mathematical properties of the NSWE-model are analysed, such as the conservation law property, hyperbolicity and boundedness of the state (four-dimensional density). In Section 6, we provide a numerical example verifying the ability of the model to predict the traffic flow evolution. Finally, the concluding remarks are given in Section 7.

2. Traffic Flow at One Intersection

The main goal of this paper is to derive a multi-directional macroscopic traffic model. To achieve this, we need, first of all, to derive a traffic flow model for **one intersection**. During this derivation we will be able to define several important variables that will be later used to derive a macroscopic continuous model. In particular, we use the CTM model [3] at one intersection to introduce the concept of *partial flows* from one road to another road, which is then used to express the directions as a function of the network topology (more details are given below). Thus, we consider an intersection located at (x_1, y_1) with two incoming and two outgoing roads (as illustrated in Fig. 1), and show a step-by-step derivation of the traffic model at this intersection, which is then generalized to an intersection with an arbitrary number of incoming and outgoing roads.

2.1. Demand-Supply Concept

In general, one of the key assumption in traffic modelling is that there is a concave relation between traffic flow ϕ and vehicle density ρ . This relation is an empirical law known as the fundamental diagram (FD) [26]. Mathematically, FD $\Phi(\rho) : [0, \rho_{max}] \rightarrow \mathbb{R}^+$ is a concave function with a unique maximum ϕ_{max} (road *capacity*) achieved at the *critical density* ρ_c , while the minimum is achieved at

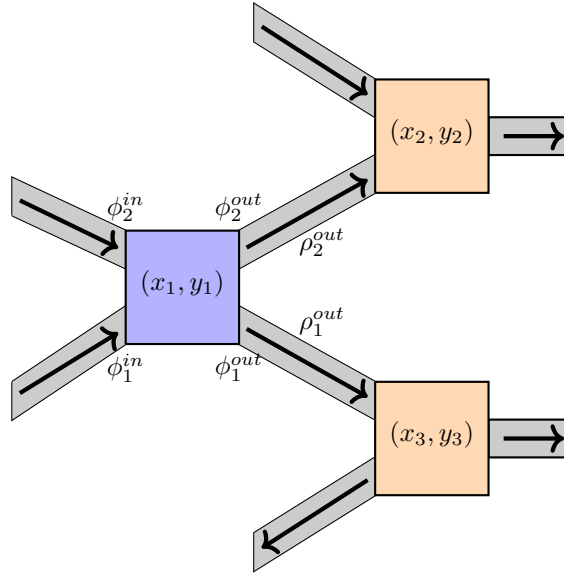


Figure 1: Example of a small traffic network consisting of 3 intersections. We consider the intersection filled in blue.

$\Phi(0) = \Phi(\rho_{max}) = 0$, i.e., for zero and *maximal density* ρ_{max} (also called the traffic jam density). If density on a road is below its critical value ρ_c , then vehicles move freely with a *positive kinematic wave speed* v , otherwise we have a congested regime characterized by a *negative kinematic wave speed* ω . Notice that the fundamental diagram parameters such as speed limits, capacities and maximal densities might vary from road to road.

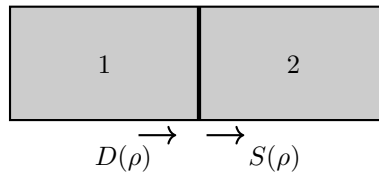


Figure 2: Schematic illustration of the demand-supply concept.

Consider a road divided into two sections as illustrated in Fig. 2. In accordance with the demand-supply concept introduced in [6], the amount of flow ϕ

that may enter section 2 from section 1 is determined by the minimum between the demand $D(\rho)$ of section 1 and the supply $S(\rho)$ of section 2:

$$\phi(\rho) = \min(D(\rho), S(\rho)), \quad \forall t \in \mathbb{R}^+, \quad (1)$$

where $D(\rho)$ and $S(\rho)$ are defined as

$$D(\rho) = \begin{cases} \phi(\rho), & \text{if } 0 \leq \rho \leq \rho_c, \\ \phi_{max}, & \text{if } \rho_c < \rho \leq \rho_{max} \end{cases} \quad (2)$$

and

$$S(\rho) = \begin{cases} \phi_{max}, & \text{if } 0 \leq \rho \leq \rho_c, \\ \phi(\rho), & \text{if } \rho_c < \rho \leq \rho_{max}. \end{cases} \quad (3)$$

2.2. Flows at Intersections: Example

We use the demand-supply concept to derive a traffic flow model for the intersection at (x_1, y_1) as illustrated in Fig. 1. In particular, we need to determine inflows and outflows, which are necessary to establish a model, since the change of the number of cars N at some location can be found, in general, as the difference between inflows and outflows, i.e.:

$$\frac{dN}{dt} = \phi^{in} - \phi^{out}.$$

Assume the fundamental diagram has a *triangular* shape as in [3]. Then in this case the demand and supply functions given in general by (2) and (3) can be defined as:

$$D(\rho) = \min(v\rho, \phi_{max}), \quad S(\rho) = \min(\omega(\rho_{max} - \rho), \phi_{max}). \quad (4)$$

Moreover, we define the critical density as $\rho_c = \rho_{max}/3$.

Throughout this paper, we use a subscript to number roads, and a superscript is used to indicate whether this particular road is incoming or outgoing, e.g., $\phi_{max,1}^{in}$ is the capacity of incoming road number 1.

Each incoming road has its own demand for the flow to enter the intersection (illustrated in Fig. 1) that reads with (4):

$$D_1^{in} = \min(v_1^{in} \rho_1^{in}, \phi_{max,1}^{in}), \quad D_2^{in} = \min(v_2^{in} \rho_2^{in}, \phi_{max,2}^{in}). \quad (5)$$

A part of the flow entering the intersection goes to the first outgoing road and the other part goes to the second outgoing road. These flows are split according to the *turning ratios* $\alpha_{ij} \in [0, 1]$, where i is the index of the incoming road and j is the index of the outgoing road. For instance, if $\alpha_{11} = 0.6$ and $\alpha_{12} = 0.4$, then 60% of the cars from the first incoming road turn to the first outgoing road, and 40% turn to the second outgoing road. Note also that the sum of turning ratios for each incoming road must be 1, i.e.,

$$\alpha_{11} + \alpha_{12} = 1, \quad \alpha_{21} + \alpha_{22} = 1.$$

The concept of turning ratios coincides with the one from the discussion on diverging intersections in [6].

Let us now introduce the concept of *partial demands*. A partial demand refers to the flow of an incoming road that wants/demands to enter a *particular* outgoing road. These are equal to the overall demands (5) multiplied by corresponding turning ratios, i.e.:

$$\begin{aligned} D_{11} &= \min(\alpha_{11} v_1^{in} \rho_1^{in}, \alpha_{11} \phi_{max,1}^{in}), & D_{12} &= \min(\alpha_{12} v_1^{in} \rho_1^{in}, \alpha_{12} \phi_{max,1}^{in}), \\ D_{21} &= \min(\alpha_{21} v_2^{in} \rho_2^{in}, \alpha_{21} \phi_{max,2}^{in}), & D_{22} &= \min(\alpha_{22} v_2^{in} \rho_2^{in}, \alpha_{22} \phi_{max,2}^{in}). \end{aligned}$$

In accordance with [6], each outgoing road provides a supply for the flow coming from intersection, which we get from (4):

$$\begin{aligned} S_1^{out} &= \min(\omega_1^{out} (\rho_{max,1}^{out} - \rho_1^{out}), \phi_{max,1}^{out}), \\ S_2^{out} &= \min(\omega_2^{out} (\rho_{max,2}^{out} - \rho_2^{out}), \phi_{max,2}^{out}). \end{aligned} \tag{6}$$

Let us also *assume* that each outgoing road has a particular supply for each incoming road, e.g., S_1^{out} is split into S_{11} and S_{21} . In order to define these *partial supplies*, we introduce *supply coefficients* $\beta_{ij} \in [0, 1]$ used to denote the supply of an outgoing road j that it provides for the maximal flow coming from a particular incoming road i (among all the incoming roads). The supply coefficient β_{ij} is thus defined as

$$\beta_{ij} = \frac{\alpha_{ij} \phi_{max,i}^{in}}{\sum_{k=1}^{n_{in}} \alpha_{kj} \phi_{max,k}^{in}}, \tag{7}$$

Notice that for each outgoing road the sum of supply coefficients must be 1, i.e.,

$$\beta_{11} + \beta_{21} = 1, \quad \beta_{12} + \beta_{22} = 1.$$

With the definition of supply coefficients (7), we are now ready to formulate partial supplies as the overall supplies given by (6) multiplied by corresponding supply coefficients:

$$S_{ij} = \beta_{ij} S_j^{out} = \min(\beta_{ij} \omega_j^{out} (\rho_{max,j}^{out} - \rho_j^{out}), \beta_{ij} \phi_{max,j}^{out}).$$

Under the assumption of supply coefficients, we can also define partial flows as the minimum between partial demand and partial supply, i.e., $\phi_{11} = \min(D_{11}, S_{11})$ yields:

$$\phi_{11} = \min(\alpha_{11} v_1^{in} \rho_1^{in}, \beta_{11} \omega_1^{out} (\rho_{max,1}^{out} - \rho_1^{out}), \alpha_{11} \phi_{max,1}^{in}, \beta_{11} \phi_{max,1}^{out}),$$

Finally, the flows of incoming and outgoing roads are found by summing up the partial flows, i.e.,

$$\begin{aligned} \phi_1^{in} &= \phi_{11} + \phi_{12}, & \phi_2^{in} &= \phi_{21} + \phi_{22}, \\ \phi_1^{out} &= \phi_{11} + \phi_{21}, & \phi_2^{out} &= \phi_{12} + \phi_{22}, \end{aligned}$$

Notice that the sum of flows before and after the intersection is always conserved, i.e., $\phi_1^{in} + \phi_2^{in} = \phi_1^{out} + \phi_2^{out}$. Thus, we have established a traffic flow model at the intersection by explicitly deriving expressions for its inflows and outflows.

2.3. Flows at Intersections: Generalization

We can generalize the calculations from the previous subsection to any intersection with n_{in} incoming roads having densities ρ_i^{in} and flows ϕ_i^{in} for $i \in \{1, \dots, n_{in}\}$ and with n_{out} outgoing roads having densities ρ_j^{out} and flows ϕ_j^{out} for $j \in \{1, \dots, n_{out}\}$.

Every incoming road i has its own demand D_i^{in} for the flow to enter the intersection:

$$D_i^{in} = \min(v_i^{in} \rho_i^{in}, \phi_{max,i}^{in}).$$

Then, we define partial demands from road i to road j as

$$D_{ij} = \alpha_{ij} D_i^{in} = \min(\alpha_{ij} v_i^{in} \rho_i^{in}, \alpha_{ij} \phi_{max,i}^{in}).$$

Supply S_j^{out} of the outgoing road j is simply given by

$$S_j^{out} = \min(\omega_j^{out}(\rho_{max,j}^{out} - \rho_j^{out}), \phi_{max,j}^{out}).$$

Partial flow ϕ_{ij} entering an outgoing road j from an incoming road i are defined as

$$\begin{aligned} \phi_{ij} &= \min(D_{ij}, S_{ij}) = \\ &= \min(\alpha_{ij} v_i^{in} \rho_i^{in}, \beta_{ij} \omega_j^{out}(\rho_{max,j}^{out} - \rho_j^{out}), \alpha_{ij} \phi_{max,i}^{in}, \beta_{ij} \phi_{max,j}^{out}). \end{aligned} \quad (8)$$

Finally, the flow from the incoming road ϕ_i^{in} is the sum over all the flows exiting this road, and the flow into outgoing road ϕ_j^{out} is the sum over all the flows coming into this road:

$$\phi_i^{in} = \sum_{j=1}^{n_{out}} \phi_{ij}, \quad \phi_j^{out} = \sum_{i=1}^{n_{in}} \phi_{ij}. \quad (9)$$

For a better overview, we have summarized all the notations introduced in this section in Appendix A.1.

3. The NSWE-framework

Our main goal is to model the evolution of multi-directional traffic in a large-scale network. The main challenge thereby is that roads at an intersection may be oriented arbitrarily. Hence, we would like to obtain a model in terms of flows that are parallel to the cardinal directions: North (**N**), South (**S**), West (**W**) and East (**E**). This will enable us to formulate the model in macroscopic terms, if every intersection will be described in a unified way. Let us call it the **NSWE**-model and denote the corresponding variables by bars, e.g., $\bar{\phi}$.

In order to formulate the traffic model in terms of NSWE, *we will use only the geometric properties of the network*, such as the angle of the roads directions with respect to the East direction denoted by θ , see Fig. 3.

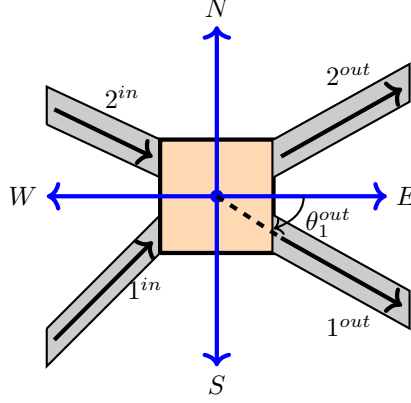


Figure 3: Main idea of NSWE-framework: map roads' directions at an intersection into four cardinal directions: North, South, West and East. Roads 1^{in} and 2^{out} are oriented towards North-East and roads 2^{in} and 1^{out} are oriented towards South-East.

Let us consider the projection of flows into the North. We calculate the flow to the North as a weighted sum of all flows on the roads which have angles less than $\pi/2$ with the North direction, i.e., these are roads 1^{in} and 2^{out} in Fig. 3. This also means that, in general, an angle of the road's direction with non-zero projection to the North is bounded to the range $\theta \in (0, \pi)$, while for non-zero projections to the South, West and East the angle must be $\theta \in (\pi, 2\pi)$, $\theta \in (\pi/2, 3\pi/2)$ and $\theta \in (0, \frac{\pi}{2}) \cup (\frac{3\pi}{2}, 2\pi)$, respectively. Then, the outflows in the NSWE-formulation are:

$$\begin{aligned}\bar{\phi}_N^{out} &= p_{\theta_1^{out}}^N \phi_1^{out} + p_{\theta_2^{out}}^N \phi_2^{out}, & \bar{\phi}_S^{out} &= p_{\theta_1^{out}}^S \phi_1^{out} + p_{\theta_2^{out}}^S \phi_2^{out}, \\ \bar{\phi}_W^{out} &= p_{\theta_1^{out}}^W \phi_1^{out} + p_{\theta_2^{out}}^W \phi_2^{out}, & \bar{\phi}_E^{out} &= p_{\theta_1^{out}}^E \phi_1^{out} + p_{\theta_2^{out}}^E \phi_2^{out},\end{aligned}$$

where $p_\theta \in [0, 1]$ are the weights that should satisfy the following properties:

1. If a road goes exactly to the North, $p_\theta^N = 1$.
2. If a road has an angle equal to or greater than $\pi/2$ with the North direction, $p_\theta^N = 0$.
3. The sum $p_\theta^N + p_\theta^S + p_\theta^W + p_\theta^E = 1$ to ensure the conservation of flows.

Notice that these properties are defined for the North direction, while the same holds also for other directions.

The simplest choice for the coefficients p_θ , satisfying all these properties, is

$$\begin{aligned}
p_\theta^N &= \begin{cases} \frac{\sin(\theta)}{|\cos(\theta)| + |\sin(\theta)|}, & \theta \in (0, \pi), \\ 0, & \text{elsewhere,} \end{cases} \\
p_\theta^S &= \begin{cases} \frac{-\sin(\theta)}{|\cos(\theta)| + |\sin(\theta)|}, & \theta \in (\pi, 2\pi), \\ 0, & \text{elsewhere,} \end{cases} \\
p_\theta^W &= \begin{cases} \frac{-\cos(\theta)}{|\cos(\theta)| + |\sin(\theta)|}, & \theta \in \left(\frac{\pi}{2}, \frac{3\pi}{2}\right), \\ 0, & \text{elsewhere,} \end{cases} \\
p_\theta^E &= \begin{cases} \frac{\cos(\theta)}{|\cos(\theta)| + |\sin(\theta)|}, & \theta \in \left(0, \frac{\pi}{2}\right) \cup \left(\frac{3\pi}{2}, 2\pi\right), \\ 0, & \text{elsewhere.} \end{cases}
\end{aligned} \tag{10}$$

where θ is a positive angle between the direction of the road and the East direction.

Notice that, in general, *each road can have non-zero weights with at most two directions*. For example, in Fig.3 the flow along the first outgoing road 1^{out} has only two non-zero weights: $p_{\theta_1^{out}}^S$ and $p_{\theta_1^{out}}^E$.

Thus, flows *at each intersection* in NSWE-formulation should be given by vectors $\bar{\phi}^{in} = (\bar{\phi}_N^{in}, \bar{\phi}_S^{in}, \bar{\phi}_W^{in}, \bar{\phi}_E^{in})^T$ and $\bar{\phi}^{out} = (\bar{\phi}_N^{out}, \bar{\phi}_S^{out}, \bar{\phi}_W^{out}, \bar{\phi}_E^{out})^T$. This allows us to establish the following relation with the flows from the original road formulation given by (9):

$$\bar{\phi}^{in} = \begin{pmatrix} \bar{\phi}_N^{in} \\ \bar{\phi}_S^{in} \\ \bar{\phi}_W^{in} \\ \bar{\phi}_E^{in} \end{pmatrix} = \begin{bmatrix} p_{\theta_1^{in}}^N & p_{\theta_2^{in}}^N \\ p_{\theta_1^{in}}^S & p_{\theta_2^{in}}^S \\ p_{\theta_1^{in}}^W & p_{\theta_2^{in}}^W \\ p_{\theta_1^{in}}^E & p_{\theta_2^{in}}^E \end{bmatrix} \begin{pmatrix} \phi_1^{in} \\ \phi_2^{in} \end{pmatrix}$$

and

$$\bar{\phi}^{out} = \begin{pmatrix} \bar{\phi}_N^{out} \\ \bar{\phi}_S^{out} \\ \bar{\phi}_W^{out} \\ \bar{\phi}_E^{out} \end{pmatrix} = \begin{bmatrix} p_{\theta_1^{out}}^N & p_{\theta_2^{out}}^N \\ p_{\theta_1^{out}}^S & p_{\theta_2^{out}}^S \\ p_{\theta_1^{out}}^W & p_{\theta_2^{out}}^W \\ p_{\theta_1^{out}}^E & p_{\theta_2^{out}}^E \end{bmatrix} \begin{pmatrix} \phi_1^{out} \\ \phi_2^{out} \end{pmatrix}.$$

For a general case of n_{in} incoming and n_{out} outgoing roads, we introduce matrices $P_{in} \in \mathbb{R}^{4 \times n_{in}}$ and $P_{out} \in \mathbb{R}^{4 \times n_{out}}$ consisting of coefficients $p_{\theta_i^{in}}$ and $p_{\theta_j^{out}}$, respectively. Thus, the flows are transformed into the NSWE-formulation as follows:

$$\bar{\phi}^{in} = P_{in}\phi^{in}, \quad \bar{\phi}^{out} = P_{out}\phi^{out}. \quad (11)$$

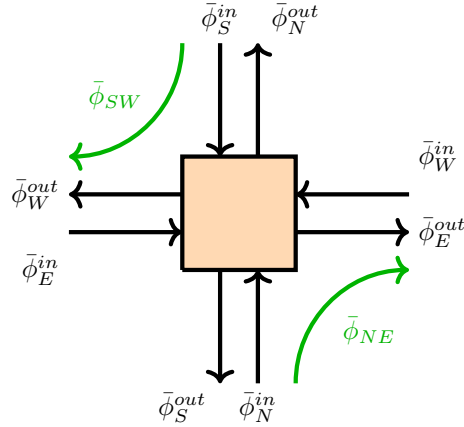


Figure 4: Explanation of flows' directions in NSWE-formulation.

In general, $\bar{\phi}_N^{in}$ is the flow on incoming roads going to the North direction (before the intersection), and $\bar{\phi}_N^{out}$ is the flow on outgoing roads going to the North (after the intersection), see Fig. 4 for illustration of this concept. They can also be represented by the sums over *partial flows in the NSWE-formulation*:

$$\bar{\phi}_N^{in} = \bar{\phi}_{NN} + \bar{\phi}_{NS} + \bar{\phi}_{NW} + \bar{\phi}_{NE}, \quad (12)$$

and

$$\bar{\phi}_N^{out} = \bar{\phi}_{NN} + \bar{\phi}_{SN} + \bar{\phi}_{WN} + \bar{\phi}_{EN}, \quad (13)$$

where, for example, $\bar{\phi}_{NE}$ is the flow consisting of cars going to the North before the intersection and to the East after they have passed the intersection, see Fig. 4. Thus, $\bar{\phi}_N^{in}$ is composed of all such flows that were going to the North before the intersection and then continued their way either to the North or changed to the South, West or East after passing the intersection.

In NSWE formulation, partial flows can be calculated as follows:

$$\bar{\phi}_{EN} = \sum_{i=1}^{n_{in}} \sum_{j=1}^{n_{out}} p_{\theta_i^{in}}^E p_{\theta_j^{out}}^N \phi_{ij}, \quad (14)$$

where p_{θ} are the NSWE weights from (10).

Notice that the correctness of this definition of partial flows can be verified by inserting (14) into (13):

$$\begin{aligned} \bar{\phi}_N^{out} &= \sum_{j=1}^{n_{out}} p_{\theta_j^{out}}^N \left[\sum_{i=1}^{n_{in}} \left(p_{\theta_i^{in}}^N + p_{\theta_i^{in}}^S + p_{\theta_i^{in}}^W + p_{\theta_i^{in}}^E \right) \phi_{ij} \right] = \\ &= \sum_{j=1}^{n_{out}} p_{\theta_j^{out}}^N \sum_{i=1}^{n_{in}} \phi_{ij} = \sum_{j=1}^{n_{out}} p_{\theta_j^{out}}^N \phi_j^{out}, \end{aligned}$$

whereby we have used the fact that the weights' sum over all the cardinal direction is 1 (see property 3 in the definition of p_{θ}) and (9).

To gain more insight into the concept of partial flows, let us consider an example of an intersection that has one incoming and one outgoing road, as shown in Fig. 5. First, we define the incoming flow in the NSWE-formulation from Fig. 5:

$$\bar{\phi}^{in} = \begin{pmatrix} \bar{\phi}_N^{in} \\ \bar{\phi}_S^{in} \\ \bar{\phi}_W^{in} \\ \bar{\phi}_E^{in} \end{pmatrix} = \begin{pmatrix} 0 \\ \bar{\phi}_{SN} + \bar{\phi}_{SE} \\ 0 \\ \bar{\phi}_{EN} + \bar{\phi}_{EE} \end{pmatrix}.$$

Then, we see that $\bar{\phi}_N^{in} = \bar{\phi}_W^{in} = 0$, since the incoming road has a zero weight with respect to both North and West direction, while it has non-zero weights

with the South and East directions. The outgoing road has non-zero weights only with North and East direction, which results into $\bar{\phi}_S^{in} = \bar{\phi}_{SN} + \bar{\phi}_{SE}$ and $\bar{\phi}_E^{in} = \bar{\phi}_{EN} + \bar{\phi}_{EE}$.

In a similar way, we analyse the flow on the outgoing road that yields:

$$\bar{\phi}^{out} = \begin{pmatrix} \bar{\phi}_N^{out} \\ \bar{\phi}_S^{out} \\ \bar{\phi}_W^{out} \\ \bar{\phi}_E^{out} \end{pmatrix} = \begin{pmatrix} \bar{\phi}_{SN} + \bar{\phi}_{EN} \\ 0 \\ 0 \\ \bar{\phi}_{SE} + \bar{\phi}_{EE} \end{pmatrix}.$$

Also note that in Figure 5 there is no flow in the West direction, therefore all the flows containing at least one W are zero, e.g., $\bar{\phi}_{NW} = \bar{\phi}_{SW} = 0$, etc.

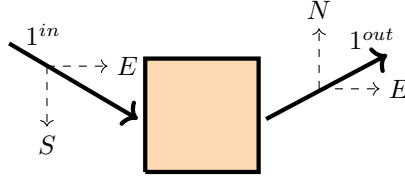


Figure 5: Sketch of an intersection with one incoming road 1^{in} and one outgoing road 1^{out} .

For a better overview, we have summarized all the notations introduced in this and next sections in Appendix A.2.

4. Derivation of the NSWE-model

Similar to our road model given by (9) and (8), we would like to define partial flows in the NSWE-formulation using the demand-supply concept (1). For this we will need to provide the NSWE-definition of the turning ratios $\bar{\alpha}$ and supply coefficients $\bar{\beta}$. Moreover, we will also have to define the fundamental diagram parameters \bar{v} , $\bar{\omega}$, $\bar{\rho}_{max}$ in NSWE-formulation to be able to derive the complete model that predicts the density evolution in four cardinal directions.

4.1. Turning Ratios and Supply Coefficients

The demand $\bar{D}^{in} \in \mathbb{R}^{4 \times 1}$ and supply $\bar{S}^{out} \in \mathbb{R}^{4 \times 1}$ functions from (4) can be formulated in terms of NSWE using coefficient matrices P_{in} , P_{out} as in (11):

$$\begin{aligned}\bar{D}^{in} &= P_{in} \min(v^{in} \rho^{in}, \phi_{max}^{in}), \\ \bar{S}^{out} &= P_{out} \min(\omega^{out} (\rho_{max}^{out} - \rho^{out}), \phi_{max}^{out}).\end{aligned}\tag{15}$$

Now, without loss of generality, let us consider the partial flow from East to North $\bar{\phi}_{EN}$, which we would like to write using demand and supply as in (8):

$$\bar{\phi}_{EN} = \min(\bar{\alpha}_{EN} \bar{D}_E^{in}, \bar{\beta}_{EN} \bar{S}_N^{out}),\tag{16}$$

where $\bar{\alpha}_{EN}$ is the turning ratio from East to North, and $\bar{\beta}_{EN}$ is the proportion of supply of the North provided for the cars arriving from the East, i.e., the same as β_{ij} from (7) but in the NSWE-formulation.

The coefficients $\bar{\alpha}_{EN}$ and $\bar{\beta}_{EN}$ need to be determined, which can be done using (14), in which we substitute (8), which yields

$$\bar{\phi}_{EN} = \sum_{i=1}^{n_{in}} \sum_{j=1}^{n_{out}} p_{\theta_i^E}^E p_{\theta_j^N}^N \min\left(\alpha_{ij} v_i^{in} \rho_i^{in}, \beta_{ij} \omega_j^{out} (\rho_{max,j}^{out} - \rho_j^{out}), \alpha_{ij} \phi_{max,i}^{in}, \beta_{ij} \phi_{max,j}^{out}\right).$$

This expression is a sum over minimum functions, which is difficult to handle. Thus, we make the following *approximation*: we change the order of taking the minimum and the summations. This leads to the minimum function over just four arguments as in demand-supply concept:

$$\bar{\phi}_{EN} \approx \min\left(\sum_{j=1}^{n_{out}} p_{\theta_j^N}^N \sum_{i=1}^{n_{in}} p_{\theta_i^E}^E \alpha_{ij} v_i^{in} \rho_i^{in}, \sum_{j=1}^{n_{out}} p_{\theta_j^N}^N \sum_{i=1}^{n_{in}} p_{\theta_i^E}^E \beta_{ij} \omega_j^{out} (\rho_{max,j}^{out} - \rho_j^{out}), \dots\right).$$

Notice that the difference between putting minimum inside and outside the summation is decreasing as the level of the homogeneity in the congestion of links increases. This approximation is exact if all roads in the network are in the same traffic regime, i.e., either all roads are in free-flow or congested.

We set the latter expression equal to (16) for $\phi = \phi_{max}$, and get the coefficients $\bar{\alpha}_{EN}$ and $\bar{\beta}_{EN}$ that read

$$\bar{\alpha}_{EN} = \frac{\sum_{j=1}^{n_{out}} \left[p_{\theta_j^N}^N \sum_{i=1}^{n_{in}} \alpha_{ij} p_{\theta_i^E}^E \phi_{max,i}^{in} \right]}{\sum_{i=1}^{n_{in}} p_{\theta_i^E}^E \phi_{max,i}^{in}},\tag{17}$$

and

$$\bar{\beta}_{EN} = \frac{\sum_{i=1}^{n_{in}} \left[p_{\theta_i^E}^E \sum_{j=1}^{n_{out}} \beta_{ij} p_{\theta_j^N}^N \phi_{max,j}^{out} \right]}{\sum_{j=1}^{n_{out}} p_{\theta_j^N}^N \phi_{max,j}^{out}}. \quad (18)$$

4.2. FD Parameters in the NSWE-framework

Consider the demand and the supply functions in the NSWE-formulation. From one side, we can calculate them using the projection matrices P_{in} and P_{out} as in (15). From the other side, we would like to be able to calculate demand and supply using a triangular FD, which should enable us to describe traffic flow in a unified way for any intersection. Recall that FD parameters depend on a specific road, while another road might already have a different speed limit or capacity.

Thus, we are going to define a unified FD in the NSWE-formulation such that the FD is defined for each direction separately. This equivalently means that the parameters of FD will all become four-dimensional vectors or 4×4 diagonal matrices. Let us consider the FD for the North direction, while similar steps should be done for other directions. That is, for \bar{D}_N and \bar{S}_N we would like to find kinematic wave speeds \bar{v}_N and $\bar{\omega}_N$ and density transformations $\bar{\rho}_N^{in}$ and $\bar{\rho}_N^{out}$ such that the following relations would hold:

$$\begin{aligned} \bar{D}_N &= \sum_{i=1}^{n_{in}} p_i^N \min(v_i \rho_i, \phi_{max,i}) \approx \min(\bar{v}_N \bar{\rho}_N^{in}, \bar{\phi}_{max,N}^{in}), \\ \bar{S}_N &= \sum_{j=1}^{n_{out}} p_j^N \min(\omega_j (\rho_{max,j} - \rho_j), \phi_{max,j}) \approx \min(\bar{\omega}_N (\bar{\rho}_{max,N}^{out} - \bar{\rho}_N^{out}), \bar{\phi}_{max,N}^{out}). \end{aligned}$$

Note that in the case when there are much more roads than cardinal directions, we can use only approximations of the fundamental diagram.

By approximating sum of minimum functions as a minimum of sums and writing the conditions on maximal flows together, we get

$$\begin{aligned} \sum_{i=1}^{n_{in}} p_i^N v_i \rho_{c,i} &= \bar{v}_N \bar{\rho}_{c,N}^{in}, \\ \sum_{j=1}^{n_{out}} p_j^N \omega_j (\rho_{max,j} - \rho_{c,j}) &= \bar{\omega}_N (\bar{\rho}_{max,N}^{out} - \bar{\rho}_{c,N}^{out}). \end{aligned} \quad (19)$$

System (19) is undetermined since it consists of two equations that have five unknowns $(\bar{v}_N, \bar{\omega}_N, \bar{\rho}_{c,N}^{in}, \bar{\rho}_{c,N}^{out}, \bar{\rho}_{max,N}^{out})$.

In general, we get the coordinates of each road, its number of lanes and speed limits as network data. The speed limits are directly related to the kinematic wave speeds v_j , while the maximal density $\rho_{max,j}$ on each road j is determined by its number of lanes and the minimal car-to-car distance (we assume it is 6m). Knowing $\rho_{max,j}$ for every road, we can easily obtain the critical density $\rho_{c,j}$ (recall that in Section 2 we assumed that $\rho_c = \rho_{max}/3$). The negative kinematic wave speeds ω_j can be obtained from the speed limits v_j and critical density $\rho_{c,j}$ as

$$\omega_j = \frac{\rho_{c,j} v_j}{\rho_{max,j} - \rho_{c,j}}.$$

Assume that the densities are transformed into the NSWE-formulation in the same way as it is done for the flows (11), e.g.:

$$\bar{\rho}_N = \sum_{i=1}^{n_{in}} p_i^N \rho_i + \sum_{j=1}^{n_{out}} p_j^N \rho_j, \quad (20)$$

which is then also done for the maximal $\bar{\rho}_{max,N}$ and critical $\bar{\rho}_{c,N}$ densities.

After we have defined all the densities, we can finally express the velocities from (19) as

$$\bar{v}_N = \frac{\sum_{i=1}^{n_{in}} p_i^N v_i \rho_{c,i} + \sum_{j=1}^{n_{out}} p_j^N v_j \rho_{c,j}}{\bar{\rho}_{c,N}},$$

$$\bar{\omega}_N = \frac{\sum_{i=1}^{n_{in}} p_i^N \omega_i (\rho_{max,i} - \rho_{c,i}) + \sum_{j=1}^{n_{out}} p_j^N \omega_j (\rho_{max,j} - \rho_{c,j})}{\bar{\rho}_{max,N} - \bar{\rho}_{c,N}}.$$

4.3. Continuation

Our main goal is to derive a macroscopic NSWE-model for multi-directional traffic in terms of density. This model is derived by considering an intersection and its outgoing roads that should be viewed as incoming roads for the neighbouring intersections. In the end, we will be able to describe the whole urban area due to a unified description of the traffic behaviour at any intersection.

This unified description will be obtained using the continuation method that was introduced in [25].

Previously, we considered inflow ϕ^{in} and outflow ϕ^{out} with respect to some intersection. However, in the following, we consider inflow and outflow with respect to roads that we will denote by ψ^{in} and ψ^{out} as in Fig. 6.

Recall that θ is an angle between the road direction and the East direction. Denote the flow in the direction θ as ψ_θ . Essentially, there are two flows with direction θ : inflow ψ_θ^{in} which is a sum of all flows incoming in a road with direction θ , and outflow ψ_θ^{out} which is a sum of all flows outgoing from this road. Notice that, in the following, we will deal with outgoing roads only, thus, we will skip the superscript in the notation of angle, i.e., $\theta_j^{out} = \theta_j$.

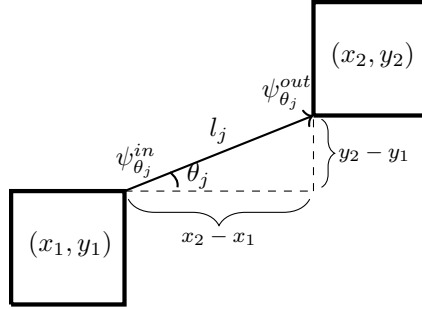


Figure 6: Illustration of the notations used for the derivation of NSWE-model.

Now consider some road j of length l_j that is an outgoing road for the intersection located at (x_1, y_1) , see Fig. 6. The density evolution on road j that is connecting the intersection at (x_1, y_1) and the intersection at (x_2, y_2) is

$$\frac{\partial \rho_j}{\partial t} = \frac{1}{l_j} \left(\psi_{\theta_j}^{in}(x_1, y_1) - \psi_{\theta_j}^{out}(x_2, y_2) \right),$$

where $\theta_j = \text{atan}[(y_2 - y_1)/(x_2 - x_1)]$ as in Fig. 6.

The equation above depends on two different space points (x_1, y_1) and (x_2, y_2) . However, we would like to obtain an equation that is described at a unique point. In order to achieve that, we can perform continuation at the beginning of the road (x_1, y_1) . Its simplest form, the continuation method corresponds to the

first order term of Taylor expansion in spatial coordinates, which reads:

$$\psi_{\theta_j}^{out}(x_2, y_2) \approx \psi_{\theta_j}^{out}(x_1, y_1) + (x_2 - x_1) \frac{\partial \psi_{\theta_j}^{out}}{\partial x} + (y_2 - y_1) \frac{\partial \psi_{\theta_j}^{out}}{\partial y},$$

and assuming this approximation to be an equality, we get the following model

$$\frac{\partial \rho_j}{\partial t} = \frac{1}{l_j} \left(\psi_{\theta_j}^{in}(x_1, y_1) - \psi_{\theta_j}^{out}(x_1, y_1) - (x_2 - x_1) \frac{\partial \psi_{\theta_j}^{out}}{\partial x} - (y_2 - y_1) \frac{\partial \psi_{\theta_j}^{out}}{\partial y} \right),$$

or simply

$$\frac{\partial \rho_j}{\partial t} = \frac{1}{l_j} \left(\psi_{\theta_j}^{in}(x_1, y_1) - \psi_{\theta_j}^{out}(x_1, y_1) \right) - \cos \theta_j \frac{\partial \psi_{\theta_j}^{out}}{\partial x} - \sin \theta_j \frac{\partial \psi_{\theta_j}^{out}}{\partial y}.$$

At the same time, by performing continuation at the end of the road (x_2, y_2) we arrive at

$$\frac{\partial \rho_j}{\partial t} = \frac{1}{l_j} \left(\psi_{\theta_j}^{in}(x_2, y_2) - \psi_{\theta_j}^{out}(x_2, y_2) \right) - \cos \theta_j \frac{\partial \psi_{\theta_j}^{in}}{\partial x} - \sin \theta_j \frac{\partial \psi_{\theta_j}^{in}}{\partial y}.$$

Since the density along the road is assumed to be constant, both continuous models can be used to represent the original one. The first model is defined in terms of the beginning of the road and contains spatial derivatives of $\psi_{\theta_j}^{out}$, whereas the second model is defined in terms of end of the road and contains spatial derivatives of $\psi_{\theta_j}^{in}$. However, performing continuation not at the end points but somewhere in between can result into a more general form.

Let us perform continuation of the model for some arbitrary point along the road (x, y) whose coordinates lie between two endpoints (x_1, y_1) and (x_2, y_2) :

$$x = x_1 \gamma + x_2 (1 - \gamma), \quad y = y_1 \gamma + y_2 (1 - \gamma),$$

where $\gamma \in [0, 1]$. Thus, by performing continuation at (x, y) , we arrive at

$$\begin{aligned} \frac{\partial \rho_j}{\partial t} = \frac{1}{l_j} \left(\psi_{\theta_j}^{in}(x, y) - \psi_{\theta_j}^{out}(x, y) \right) - \cos \theta_j \frac{\partial((1 - \gamma)\psi_{\theta_j}^{in} + \gamma\psi_{\theta_j}^{out})}{\partial x} \\ - \sin \theta_j \frac{\partial((1 - \gamma)\psi_{\theta_j}^{in} + \gamma\psi_{\theta_j}^{out})}{\partial y}. \end{aligned} \quad (21)$$

Now let the vector-flow on road j be

$$\vec{\Psi}_{\theta_j} = \psi_{\theta_j} \begin{pmatrix} \cos \theta_j \\ \sin \theta_j \end{pmatrix}, \quad \text{where } \psi_{\theta_j} = (1 - \gamma)\psi_{\theta_j}^{in} + \gamma\psi_{\theta_j}^{out}.$$

Then, the model (21) can be rewritten as

$$\frac{\partial \rho_j}{\partial t} = \frac{1}{l_j} \left(\psi_{\theta_j}^{in}(x, y) - \psi_{\theta_j}^{out}(x, y) \right) - \nabla \cdot \vec{\Psi}_{\theta_j}(x, y), \quad (22)$$

where ∇ is a nabla operator defined as $\nabla = \left(\frac{\partial}{\partial x}, \frac{\partial}{\partial y} \right)^T$.

This model (22) predicts the dynamics of the vehicles' density at some outgoing road j with direction θ . Note that this equation (22) has the same form for any intersection located at (x_k, y_k) , where $k \in [1, \dots, N]$ is an index used to label intersections in the domain of interest. Notice that parameter γ was introduced only for the derivation purposes, it will not explicitly appear in the final model, see the details below.

4.4. The NSWE-model

We would like to translate the model (22) given in terms of roads into NSWE-formulation. Recall that the densities in every direction are transformed similar to (20). Let us again consider the North direction for simplicity, while the same steps should be performed for all other directions.

Thus, multiplying the equation (22) by $p_{\theta_j}^N$ and taking the summation, we get the model of the vehicle density that evolves in the North direction on outgoing roads of an intersection located at (x_k, y_k) that reads

$$\frac{\partial \bar{\rho}_N}{\partial t} = \sum_{j=1}^{n_{out}} p_{\theta_j}^N \frac{1}{l_j} \left(\psi_{\theta_j}^{in} - \psi_{\theta_j}^{out} \right) - \nabla \cdot \left(\sum_{j=1}^{n_{out}} p_{\theta_j}^N \vec{\Psi}_{\theta_j} \right). \quad (23)$$

We cannot further simplify the equation (23) towards the NSWE-formulation, since the summations contain additional index-dependent coefficients such as $1/l_j$, $\sin \theta_j$ and $\cos \theta_j$.

Let us then approximate the system (23) by averaging road's length l_j :

$$L = \frac{\sum_{j=1}^{n_{out}} \rho_{max,j} l_j}{\sum_{j=1}^{n_{out}} \rho_{max,j}},$$

such that the mean length of outgoing roads conserves the maximum number of cars. Further, we also approximate sine and cosine in (23) as

$$\overline{\cos \theta_N} = \frac{\sum_{j=1}^{n_{out}} p_{\theta_j}^N \cos \theta_j \psi_{max,j}}{\sum_{j=1}^{n_{out}} p_{\theta_j}^N \psi_{max,j}}, \quad \overline{\sin \theta_N} = \frac{\sum_{j=1}^{n_{out}} p_{\theta_j}^N \sin \theta_j \psi_{max,j}}{\sum_{j=1}^{n_{out}} p_{\theta_j}^N \psi_{max,j}}.$$

Substituting these approximations into (23), we get

$$\begin{aligned} \frac{\partial \bar{\rho}_N}{\partial t} &= \frac{1}{L} \sum_{j=1}^{n_{out}} p_{\theta_j}^N (\psi_{\theta_j}^{in} - \psi_{\theta_j}^{out}) - \\ &\quad - \nabla \cdot \left(\sum_{j=1}^{n_{out}} \left(\frac{\overline{\cos \theta_N}}{\overline{\sin \theta_N}} \right) p_{\theta_j}^N ((1 - \gamma) \psi_{\theta_j}^{in} + \gamma \psi_{\theta_j}^{out}) \right), \end{aligned}$$

or simply

$$\frac{\partial \bar{\rho}_N}{\partial t} = \frac{1}{L} (\bar{\psi}_N^{in} - \bar{\psi}_N^{out}) - \nabla \cdot \left(\left(\frac{\overline{\cos \theta_N}}{\overline{\sin \theta_N}} \right) ((1 - \gamma) \bar{\psi}_N^{in} + \gamma \bar{\psi}_N^{out}) \right), \quad (24)$$

where we can further define $\bar{\psi}_N = (1 - \gamma) \bar{\psi}_N^{in} + \gamma \bar{\psi}_N^{out}$.

Notice that this model (24) is a macroscopic NSWE-model (thus, it does not depend on road index j any more). However, it can be further simplified in order to get rid of derivatives over multi-directional flows, since otherwise the model can lose hyperbolicity and, moreover, we want to get rid of parameter γ .

4.5. Model Simplification

The term under the space derivative is $\bar{\psi}_N = (1 - \gamma) \bar{\psi}_N^{in} + \gamma \bar{\psi}_N^{out}$. Recall that

$$\begin{aligned} \bar{\psi}_N^{in} &= \bar{\psi}_{NN} + \bar{\psi}_{SN} + \bar{\psi}_{WN} + \bar{\psi}_{EN}, \\ \bar{\psi}_N^{out} &= \bar{\psi}_{NN} + \bar{\psi}_{NS} + \bar{\psi}_{NW} + \bar{\psi}_{NE}, \end{aligned}$$

which is the same as in (12) and (13) but defined for $\bar{\psi}$ that we use to denote the flow w.r.t. roads. Therefore,

$$\begin{aligned} \bar{\psi}_N &= \bar{\psi}_{NN} + [(1 - \gamma) \bar{\psi}_{SN} + \gamma \bar{\psi}_{NS}] + \\ &\quad + [(1 - \gamma) \bar{\psi}_{WN} + \gamma \bar{\psi}_{NW}] + [(1 - \gamma) \bar{\psi}_{EN} + \gamma \bar{\psi}_{NE}]. \end{aligned} \quad (25)$$

Our model (24) would be considerably simplified if each term under the spatial derivative could be written only as a function of demand and supply of the corresponding direction, i.e.,

$$\bar{\psi}_N = \min(\bar{D}_N, \bar{S}_N). \quad (26)$$

Now we make an *assumption that the network is well-designed in terms of maximal flows*, that is

$$\bar{\alpha}_{NE} \bar{\psi}_{max,N} = \bar{\beta}_{NE} \bar{\psi}_{max,E}. \quad (27)$$

Physically, this assumption means that if vehicles before the intersection move at maximal possible flow, then after the intersection they continue to use the roads' capacity at maximum.

The proof that (26) holds under the assumption of a well-designed network (27), being rather technical, is shifted to Appendix B, where we show that there exists γ such that (26) holds. Thus, the transported term under the derivative in (24) can be approximated by a standard flow in the demand-supply formulation that depends only on the density of the same direction. Hence, the full system of equations is given by

$$\begin{cases} \frac{\partial \bar{\rho}_N}{\partial t} = \frac{1}{L} (\bar{\psi}_N^{in} - \bar{\psi}_N^{out}) - \frac{\partial(\overline{\cos \theta}_N \bar{\psi}_N)}{\partial x} - \frac{\partial(\overline{\sin \theta}_N \bar{\psi}_N)}{\partial y}, \\ \frac{\partial \bar{\rho}_S}{\partial t} = \frac{1}{L} (\bar{\psi}_S^{in} - \bar{\psi}_S^{out}) - \frac{\partial(\overline{\cos \theta}_S \bar{\psi}_S)}{\partial x} - \frac{\partial(\overline{\sin \theta}_S \bar{\psi}_S)}{\partial y}, \\ \frac{\partial \bar{\rho}_W}{\partial t} = \frac{1}{L} (\bar{\psi}_W^{in} - \bar{\psi}_W^{out}) - \frac{\partial(\overline{\cos \theta}_W \bar{\psi}_W)}{\partial x} - \frac{\partial(\overline{\sin \theta}_W \bar{\psi}_W)}{\partial y}, \\ \frac{\partial \bar{\rho}_E}{\partial t} = \frac{1}{L} (\bar{\psi}_E^{in} - \bar{\psi}_E^{out}) - \frac{\partial(\overline{\cos \theta}_E \bar{\psi}_E)}{\partial x} - \frac{\partial(\overline{\sin \theta}_E \bar{\psi}_E)}{\partial y}, \end{cases} \quad (28)$$

where $\bar{\psi}^{in} - \bar{\psi}^{out}$ are defined as

$$\begin{pmatrix} \bar{\psi}_N^{in} - \bar{\psi}_N^{out} \\ \bar{\psi}_S^{in} - \bar{\psi}_S^{out} \\ \bar{\psi}_W^{in} - \bar{\psi}_W^{out} \\ \bar{\psi}_E^{in} - \bar{\psi}_E^{out} \end{pmatrix} = \begin{pmatrix} \bar{\psi}_{SN} + \bar{\psi}_{WN} + \bar{\psi}_{EN} - \bar{\psi}_{NS} - \bar{\psi}_{NW} - \bar{\psi}_{NE} \\ \bar{\psi}_{NS} + \bar{\psi}_{WS} + \bar{\psi}_{ES} - \bar{\psi}_{SN} - \bar{\psi}_{SW} - \bar{\psi}_{SE} \\ \bar{\psi}_{NW} + \bar{\psi}_{SW} + \bar{\psi}_{EW} - \bar{\psi}_{WN} - \bar{\psi}_{WS} - \bar{\psi}_{WE} \\ \bar{\psi}_{NE} + \bar{\psi}_{SE} + \bar{\psi}_{WE} - \bar{\psi}_{EN} - \bar{\psi}_{ES} - \bar{\psi}_{EW} \end{pmatrix}.$$

This system of equations describes the density evolution in the vicinity of one intersection. Thus, the density $\bar{\rho}(x, y, t)$ and the flow $\bar{\psi}(x, y, t)$ are space- and

time-dependent functions, whereas all the parameters are constant ($\bar{\alpha}$, $\bar{\beta}$, L , \bar{v} , $\bar{\omega}$, $\bar{\rho}_{max}$, $\overline{\cos \theta}$, $\overline{\sin \theta}$).

Notice that the term $\bar{\psi}^{in} - \bar{\psi}^{out}$ is responsible for mixing between different density layers, e.g., $\bar{\psi}_N^{in} = \bar{\psi}_{SN} + \bar{\psi}_{WN} + \bar{\psi}_{EN}$ accounts for vehicles that were moving to the South, West and East, and then turned to the North.

System (28) together with four-dimensional fundamental diagram relating flow and density represents the **NSWE-model**, which is the main result of this paper. It models the evolution of vehicle density on outgoing roads of an intersection in all cardinal directions: North, South, West and East. The last step here is to obtain a continuous PDE system describing traffic flow propagation in the *whole network* under consideration, the parameters of system (28) should now be interpolated over the whole continuum domain. First, we calculate $\bar{\alpha}$, $\bar{\beta}$, L , \bar{v} , $\bar{\omega}$, $\bar{\rho}_{max}$, $\overline{\cos \theta}$, $\overline{\sin \theta}$ for all N intersections in the network. Then, we are looking for functions that approximate those parameters over the space, e.g., the value of an average road length can be defined $\forall(x, y) \in R^2$

$$L(x, y) = \frac{\sum_{k=1}^N L(x_k, y_k) e^{-\eta \sqrt{(x-x_k)^2 + (y-y_k)^2}}}{\sum_{k=1}^N e^{-\eta \sqrt{(x-x_k)^2 + (y-y_k)^2}}}, \quad (29)$$

where η is a weighting parameter used to denote the sensitivity of the estimated variables to the distance from the real roads. This approximation method is called Inverse Distance Weighting, where we chose an exponential function to give more weights to close roads, see [21].

Thus, we define all the variables $\forall(x, y)$, and we obtain a continuous PDE system that looks like (28) with time- and space-dependent density $\bar{\rho}(x, y, t)$ and flow $\bar{\psi}(x, y, \bar{\rho})$, while all parameters are obtained using (29), which makes them space-dependent functions, i.e., $\bar{\alpha}(x, y)$, $\bar{\beta}(x, y)$, $\bar{v}(x, y)$, etc.

4.6. Extended Model with Source Terms

In an urban network of finite size there exist roads through which cars can enter or exit the domain. Such roads are called sources and sinks, respectively. It appears that they can be trivially captured by the NSWE-model. Let us now

show how sources are implemented into system (28), while the implementation of sinks can be done in the same way.

We consider some road j , at the beginning of which cars are assumed to be created as a constant flow $\psi_{\theta_j}^{source}$. We can take this flow into account by adding it into equation (22) for road j , which yields

$$\frac{\partial \rho_j}{\partial t} = \frac{1}{l_j} (\psi_{\theta_j}^{in} - \psi_{\theta_j}^{out}) - \nabla \cdot \vec{\Psi}_{\theta_j} + \frac{1}{l_j} \psi_{\theta_j}^{source}. \quad (30)$$

In general, when we want to specify inflow for some road, we can only formulate it in terms of demand function. Then, the amount of flow that can enter this road, depends on supply that is determined by the traffic state of the road:

$$\psi_{\theta_j}^{source} = \min(D_{\theta_j}^{source}, S_{\theta_j}(\rho_j)).$$

We can rewrite (30) in NSWE-formulation by performing the transformations described in Section 4.4, which leads us to the extended NSWE-model (with sinks also included):

$$\begin{cases} \frac{\partial \bar{\rho}_N}{\partial t} = \frac{1}{L} (\bar{\psi}_N^{in} - \bar{\psi}_N^{out} + \bar{\psi}_N^{source} - \bar{\psi}_N^{sink}) - \frac{\partial(\overline{\cos \theta_N \bar{\psi}_N})}{\partial x} - \frac{\partial(\overline{\sin \theta_N \bar{\psi}_N})}{\partial y}, \\ \frac{\partial \bar{\rho}_S}{\partial t} = \frac{1}{L} (\bar{\psi}_S^{in} - \bar{\psi}_S^{out} + \bar{\psi}_S^{source} - \bar{\psi}_S^{sink}) - \frac{\partial(\overline{\cos \theta_S \bar{\psi}_S})}{\partial x} - \frac{\partial(\overline{\sin \theta_S \bar{\psi}_S})}{\partial y}, \\ \frac{\partial \bar{\rho}_W}{\partial t} = \frac{1}{L} (\bar{\psi}_W^{in} - \bar{\psi}_W^{out} + \bar{\psi}_W^{source} - \bar{\psi}_W^{sink}) - \frac{\partial(\overline{\cos \theta_W \bar{\psi}_W})}{\partial x} - \frac{\partial(\overline{\sin \theta_W \bar{\psi}_W})}{\partial y}, \\ \frac{\partial \bar{\rho}_E}{\partial t} = \frac{1}{L} (\bar{\psi}_E^{in} - \bar{\psi}_E^{out} + \bar{\psi}_E^{source} - \bar{\psi}_E^{sink}) - \frac{\partial(\overline{\cos \theta_E \bar{\psi}_E})}{\partial x} - \frac{\partial(\overline{\sin \theta_E \bar{\psi}_E})}{\partial y}, \end{cases} \quad (31)$$

where

$$\bar{\psi}_N^{source} = \min(\bar{D}_N^{source}, \bar{S}_N), \quad \bar{\psi}_N^{sink} = \min(\bar{D}_N, \bar{S}_N^{sink}),$$

with

$$\bar{D}_N^{source} = \sum_{j=1}^{n_{out}} p_{\theta_j}^N D_{\theta_j}^{source}, \quad \bar{S}_N^{sink} = \sum_{j=1}^{n_{out}} p_{\theta_j}^N S_{\theta_j}^{sink}.$$

Further, one needs to approximate \bar{D}_N^{source} and \bar{S}_N^{sink} in the whole domain, since originally we specify it in terms of roads of the network. In contrast to all other variables obtained by (29), the overall number of incoming cars should be conserved. Thus, we choose Gaussian kernel for the approximation of demand

and supply functions:

$$\bar{D}_N^{source}(x, y) = \sum_{k=1}^N \bar{D}_N^{source}(x_k, y_k) G_\sigma(x - x_k, y - y_k),$$

where $G_\sigma(x, y)$ is a two-dimensional symmetric Gaussian kernel with variance σ^2 :

$$G_\sigma(x, y) = \frac{1}{2\pi\sigma^2} e^{-\frac{1}{2\sigma^2}(x^2+y^2)}.$$

Note that such a choice of $G_\sigma(x, y)$ provides that its integral over the whole domain equals 1, therefore the overall incoming demand in (31) is the same as in the original network model (30) (road formulation).

5. Mathematical Properties of NSWE-model

Let us here study the properties of the NSWE-model. For its explicit analysis, we take system (28) that does not include any source terms. In this section we will check whether our system represents a conservation law, then we will discuss the boundedness of its state $\bar{\rho}$, and, finally, we will show that our model represents a hyperbolic PDE system.

5.1. Conservation Law

The overall density in the network is the sum over the density in all four directions, that is

$$\bar{\rho} = \bar{\rho}_N + \bar{\rho}_S + \bar{\rho}_W + \bar{\rho}_E.$$

By taking its time derivative we get

$$\frac{\partial \bar{\rho}}{\partial t} = \frac{\partial \bar{\rho}_N}{\partial t} + \frac{\partial \bar{\rho}_S}{\partial t} + \frac{\partial \bar{\rho}_W}{\partial t} + \frac{\partial \bar{\rho}_E}{\partial t},$$

for which we can substitute the equations from our model (28). It appears that all the mixing terms cancel each other, and we simply get:

$$\frac{\partial \bar{\rho}}{\partial t} = -\nabla \cdot \bar{\Psi}, \tag{32}$$

where

$$\bar{\Psi} = \left(\frac{\overline{\cos \theta_N}}{\overline{\sin \theta_N}} \right) \bar{\psi}_N + \left(\frac{\overline{\cos \theta_S}}{\overline{\sin \theta_S}} \right) \bar{\psi}_S + \left(\frac{\overline{\cos \theta_W}}{\overline{\sin \theta_W}} \right) \bar{\psi}_W + \left(\frac{\overline{\cos \theta_E}}{\overline{\sin \theta_E}} \right) \bar{\psi}_E,$$

which has a form of a conservation law, where the conserved quantity is the overall density in the network.

5.2. Boundedness of $\bar{\rho}$

The boundedness of the density $\bar{\rho} \in [0, \bar{\rho}_{max}]$ is not violated in our model given by (28), since the terms under the derivatives are resolved using the standard Godunov scheme (same as LWR). For example, consider the North direction, then the term under the derivative is just

$$\bar{\psi}_N = \min(\bar{D}_N, \bar{S}_N).$$

The mixing terms that are positive (these are $\bar{\psi}_{SN}$, $\bar{\psi}_{WN}$ and $\bar{\psi}_{EN}$ in the equation for $\bar{\rho}_N$) depend on the supply of N , e.g.,

$$\bar{\psi}_{EN} = \min(\bar{\alpha}_{EN} \bar{D}_E, \bar{\beta}_{EN} \bar{S}_N).$$

If $\bar{\rho}_N = \bar{\rho}_{max,N}$, then

$$\bar{S}_N = 0 \Rightarrow \bar{\psi}_{EN} = 0 \Rightarrow \frac{\partial \bar{\rho}_N}{\partial t} \leq 0,$$

which means that positive terms can not contribute to the increase of density when it has reached $\bar{\rho}_{max,N}$.

Negative terms depend on the demand of the North, e.g.,

$$\bar{\psi}_{NE} = \min(\bar{\alpha}_{NE} \bar{D}_N, \bar{\beta}_{NE} \bar{S}_E),$$

which in case of $\bar{\rho}_N = 0 \Rightarrow \bar{D}_N = 0$ yields:

$$\bar{\psi}_{NE} = 0 \Rightarrow \frac{\partial \bar{\rho}_N}{\partial t} \geq 0,$$

which means that negative terms do not contribute to the decrease of density when it is already zero.

5.3. Hyperbolicity

Let us now investigate whether our new continuous model (28) is hyperbolic. This is a fundamental property determining the behaviour of solutions. Thus, in contrast to other types of partial differential equations, in a hyperbolic PDE, any disturbance made in the initial data will travel along the characteristics of the equation with a finite propagation speed. Although the definition of hyperbolicity is fundamentally a qualitative one, there are precise criteria using which we can classify a partial differential equation as a hyperbolic one. In this section, we will apply this criteria to determine hyperbolicity of our model (28). Equation (28) can take the following general form:

$$\partial_t \bar{\rho} + \partial_x [F^x(\bar{\rho}, x, y)] + \partial_y [F^y(\bar{\rho}, x, y)] = g(\bar{\rho}, x, y), \quad (33)$$

where F^x and F^y are the flow matrices defined from (28) as

$$F^x = \begin{bmatrix} \overline{\cos \theta}_N \bar{\psi}_N & 0 & 0 & 0 \\ 0 & \overline{\cos \theta}_S \bar{\psi}_S & 0 & 0 \\ 0 & 0 & \overline{\cos \theta}_W \bar{\psi}_W & 0 \\ 0 & 0 & 0 & \overline{\cos \theta}_E \bar{\psi}_E \end{bmatrix},$$

and

$$F^y = \begin{bmatrix} \overline{\sin \theta}_N \bar{\psi}_N & 0 & 0 & 0 \\ 0 & \overline{\sin \theta}_S \bar{\psi}_S & 0 & 0 \\ 0 & 0 & \overline{\sin \theta}_W \bar{\psi}_W & 0 \\ 0 & 0 & 0 & \overline{\sin \theta}_E \bar{\psi}_E \end{bmatrix}.$$

The right-hand side term $g(\bar{\rho}, x, y)$ from (33) corresponds to the vector containing all the mixing terms from (28):

$$g(\bar{\rho}, x, y) = \frac{1}{L} \begin{pmatrix} \bar{\psi}_{SN} + \bar{\psi}_{WN} + \bar{\psi}_{EN} - \bar{\psi}_{NS} - \bar{\psi}_{NW} - \bar{\psi}_{NE} \\ \bar{\psi}_{NS} + \bar{\psi}_{WS} + \bar{\psi}_{ES} - \bar{\psi}_{SN} - \bar{\psi}_{SW} - \bar{\psi}_{SE} \\ \bar{\psi}_{NW} + \bar{\psi}_{SW} + \bar{\psi}_{EW} - \bar{\psi}_{WN} - \bar{\psi}_{WS} - \bar{\psi}_{WE} \\ \bar{\psi}_{NE} + \bar{\psi}_{SE} + \bar{\psi}_{WE} - \bar{\psi}_{EN} - \bar{\psi}_{EN} - \bar{\psi}_{EW} \end{pmatrix}.$$

The spatial derivatives of flow matrices from (33) can be written as

$$\begin{aligned}\partial_x[F^x(\bar{\rho}, x, y)] &= \partial_{\bar{\rho}}F^x(\bar{\rho}, x, y) \cdot \partial_x\bar{\rho} + \partial_xF^x(\bar{\rho}, x, y), \quad \text{and} \\ \partial_y[F^y(\bar{\rho}, x, y)] &= \partial_{\bar{\rho}}F^y(\bar{\rho}, x, y) \cdot \partial_y\bar{\rho} + \partial_yF^y(\bar{\rho}, x, y),\end{aligned}$$

which is further inserted into equation (33) that yields:

$$\partial_t\bar{\rho} + \partial_{\bar{\rho}}F^x(\bar{\rho}, x, y) \cdot \partial_x\bar{\rho} + \partial_{\bar{\rho}}F^y(\bar{\rho}, x, y) \cdot \partial_y\bar{\rho} = b(\bar{\rho}, x, y), \quad (34)$$

where $b(\bar{\rho}, x, y) = g(\bar{\rho}, x, y) - \partial_xF^x(\bar{\rho}, x, y) - \partial_yF^y(\bar{\rho}, x, y)$.

According to Section 3.1 of [27], the right-hand side part of (34) $b(\bar{\rho}, x, y)$ does not play any significant role for the analysis. Thus, we simply omit it by setting $b(\bar{\rho}) = 0$.

Let us further rewrite (34) as

$$\partial_t\bar{\rho} + A^x\partial_x\bar{\rho} + A^y\partial_y\bar{\rho} = 0, \quad (35)$$

where $A^x = \partial F^x/\partial\bar{\rho}$ and $A^y = \partial F^y/\partial\bar{\rho}$ represent matrices of flow derivatives:

$$A^x = \begin{bmatrix} \overline{\cos\theta}_N \frac{\partial\bar{\psi}_N}{\partial\bar{\rho}} & 0 & 0 & 0 \\ 0 & \overline{\cos\theta}_S \frac{\partial\bar{\psi}_S}{\partial\bar{\rho}} & 0 & 0 \\ 0 & 0 & \overline{\cos\theta}_W \frac{\partial\bar{\psi}_W}{\partial\bar{\rho}} & 0 \\ 0 & 0 & 0 & \overline{\cos\theta}_E \frac{\partial\bar{\psi}_E}{\partial\bar{\rho}} \end{bmatrix},$$

and

$$A^y = \begin{bmatrix} \overline{\sin\theta}_N \frac{\partial\bar{\psi}_N}{\partial\bar{\rho}} & 0 & 0 & 0 \\ 0 & \overline{\sin\theta}_S \frac{\partial\bar{\psi}_S}{\partial\bar{\rho}} & 0 & 0 \\ 0 & 0 & \overline{\sin\theta}_W \frac{\partial\bar{\psi}_W}{\partial\bar{\rho}} & 0 \\ 0 & 0 & 0 & \overline{\sin\theta}_E \frac{\partial\bar{\psi}_E}{\partial\bar{\rho}} \end{bmatrix}.$$

The system (35) is symmetrisable hyperbolic, since matrices A^x and A^y are both symmetric. This implies that the system (35) is hyperbolic [27], which equivalently means that our model given by (28) is a hyperbolic one.

6. Model Validation

To validate the theoretical results, we will compare the density predicted by the numerical simulation of NSW-model given by (28) with the results pre-

dicted by commercial software Aimsun, and then also using the results obtained from real-life measurements.



(a) Google satellite view

(b) Network in Aimsun

Figure 7: Selected area in Grenoble downtown.

6.1. Numerical Scheme

As a network we take an area located in Grenoble downtown, France, with a total surface of around $M = 1.4 \times 1 \text{ km}^2$, see Fig.7a) for the Google satellite view and Fig.7b) for the network model in Aimsun of this area.

We set the plane interval Ω divided into $N_x = 60$ cells of size $\Delta x = M/N_x$ and $N_y = 60$ cells of size $\Delta y = M/N_y$, i.e., the 2D plane is divided into 3600 cells. The mesh sizes Δx , Δy and the time step Δt are chosen such that the CFL condition is not violated [28]. The discrete density is then $\bar{\rho}^k(i, j) = (\bar{\rho}_N^k(i, j), \bar{\rho}_S^k(i, j), \bar{\rho}_W^k(i, j), \bar{\rho}_E^k(i, j))^T$, where $(i, j) \in \{1, \dots, N_x\} \times \{1, \dots, N_y\}$ is the cell index, and $k \in \mathbb{Z}^+$ is the time index.

For the numerical simulation of (28), we use the Godunov scheme [29] in two dimensions. The density in each direction $q = \{N, S, W, E\}$ is updated at every time step $\forall (i, j) \in \{1, \dots, N_x\} \times \{1, \dots, N_y\}$ as

$$\bar{\rho}_q^{k+1}(i, j) = \bar{\rho}_q^k(i, j) + \Delta t \left[E_q^k(i, j) + F_{x,q}^k(i, j) + F_{y,q}^k(i, j) + H_q^k(i, j) \right],$$

where $E_q^k(i, j)$ is the mixing term between direction layers given by

$$E_q^k(i, j) = \frac{1}{L(i, j)} \sum_{\substack{r=1 \\ r \neq q}}^4 \left(\min(\bar{\alpha}_{rq}(i, j) \bar{D}_r^k(i, j), \bar{\beta}_{rq}(i, j) \bar{S}_q^k(i, j)) \right. \\ \left. - \min(\bar{\alpha}_{qr}(i, j) \bar{D}_q^k(i, j), \bar{\beta}_{qr}(i, j) \bar{S}_r^k(i, j)) \right),$$

and $F_{x,q}^k(i, j)$, $F_{y,q}^k(i, j)$ are the derivative terms computed as:

$$F_{x,q}^k(i, j) = \frac{\overline{\cos \theta}_q(i, j) + \overline{\cos \theta}_q(i-1, j)}{2\Delta x} \min(\bar{D}_q^k(i-1, j), \bar{S}_q^k(i, j)) \\ - \frac{\overline{\cos \theta}_q(i, j) + \overline{\cos \theta}_q(i+1, j)}{2\Delta x} \min(\bar{D}_q^k(i, j), \bar{S}_q^k(i+1, j)), \\ F_{y,q}^k(i, j) = \frac{\overline{\sin \theta}_q(i, j) + \overline{\sin \theta}_q(i, j-1)}{2\Delta y} \min(\bar{D}_q^k(i, j-1), \bar{S}_q^k(i, j)) \\ - \frac{\overline{\sin \theta}_q(i, j) + \overline{\sin \theta}_q(i, j+1)}{2\Delta y} \min(\bar{D}_q^k(i, j), \bar{S}_q^k(i, j+1)).$$

Notice that $F_{x,q}^k(i, j)$, $F_{y,q}^k(i, j)$ are obtained using the upwind scheme [30] for $\overline{\cos \theta}_q(i, j) > 0$, $\overline{\sin \theta}_q(i, j) > 0$. The upwind scheme is used to guarantee the correct direction of information propagation in a flow field, which needs to be reversed if $\overline{\cos \theta}_q(i, j) < 0$ for $F_{x,q}^k(i, j)$ and $\overline{\sin \theta}_q(i, j) < 0$ for $F_{y,q}^k(i, j)$.

Finally, $H_q^k(i, j)$ includes source and sink terms, thus it is computed as

$$H_q^k(i, j) = \frac{1}{L(i, j)} \left(\min(\bar{D}_q^{source,k}(i, j), \bar{S}_q^k(i, j)) - \min(\bar{D}_q^k(i, j), \bar{S}_q^{sink,k}(i, j)) \right).$$

6.2. The SSIM Index

In order to enable a quantitative comparison between two density distributions, we use the Structural Similarity Index (SSIM) [31]. This index is usually used to measure the similarity between two images. Thereby, three different image properties are compared: luminance, contrast and structure. The SSIM index between two density distributions $\bar{\rho}_1(i, j)$ (NSWE) and $\bar{\rho}_2(i, j)$ (reference distribution from either Aimsun or real-life) $\forall (i, j) \in \{1, \dots, N_x\} \times \{1, \dots, N_y\}$ can be in general calculated as:

$$SSIM(\bar{\rho}_1, \bar{\rho}_2) = \frac{(2\mu_1\mu_2 + c)(2\sigma_{12} + c)}{(\mu_1^2 + \mu_2^2 + c)(\sigma_1^2 + \sigma_2^2 + c)}, \quad (36)$$

where μ_1 and μ_2 are the mean values of distributions $\bar{\rho}_1$ and $\bar{\rho}_2$ over the domain that are computed as:

$$\mu(\bar{\rho}) = \frac{1}{N_x} \frac{1}{N_y} \sum_{q=N}^E \sum_{i=1}^{N_x} \sum_{j=1}^{N_y} \bar{\rho}_q(i, j). \quad (37)$$

This term is used to compare luminance of two images. Then, σ_1 and σ_2 in (36) are the standard deviations of the density distributions used to compare the signal contrasts:

$$\sigma(\bar{\rho}) = \sqrt{\frac{1}{N_x} \frac{1}{N_y} \sum_{i=1}^{N_x} \sum_{j=1}^{N_y} \left(\sum_{q=N}^E \bar{\rho}_q(i, j) - \mu(\bar{\rho}) \right)^2},$$

and σ_{12} is the correlation coefficient of two density distributions used to measure the similarity of their structures:

$$\sigma(\bar{\rho}_1, \bar{\rho}_2) = \frac{1}{N_x} \frac{1}{N_y} \sum_{i=1}^{N_x} \sum_{j=1}^{N_y} \left(\sum_{q=N}^E \bar{\rho}_{q,1}(i, j) - \mu_1 \right) \left(\sum_{q=N}^E \bar{\rho}_{q,2}(i, j) - \mu_2 \right).$$

Finally, $c > 0$ in (36) is a constant that needs to be small, e.g., we take $c = 1 \cdot 10^{-13}$ for the computation. This constant prevents instability, when the denominator is close to zero. The range of SSIM is $[-1, 1]$, where 1 is achieved if two images are identical, whereas -1 means that one image is the inverse of the second image.

The main advantage of SSIM is that it is a perception-based metric used to perceive structural changes in the image, while, for example, the mean square error evaluates only the absolute error. Thus, even if two density distributions are characterized to have the same number of cars, the SSIM index is still able to detect if congested zones have different shapes.

6.3. Model Validation with Aimsun

We run a scenario of congestion formation in the selected area of Grenoble downtown (see Fig. 7). For this, we use microsimulator Aimsun and numerical simulation of NSWE-model, and then the obtained steady states are compared.

Aimsun takes network, turning ratios and inflows as input, and produces microsimulations of vehicles' trajectories. We then reconstruct the density distribution from vehicles' positions predicted by Aimsun and compare it to the state predicted by NSWE-model.

In general, we have access to the following network data: (x, y) coordinates of all intersections and its corresponding roads, as well as speed limits and number of lanes for each road. Using these data, we compute the parameters of the fundamental diagram \bar{v} , $\bar{\omega}$, $\bar{\rho}_{max}$ and the intersection parameters $\bar{\alpha}$, $\bar{\beta}$, L , $\overline{\cos \theta}$, $\overline{\sin \theta}$ in the NSWE-framework for all the intersections as follows.

For each road we read the free-flow velocity v_j from the speed limit data. Then, the maximal density $\rho_{max,j}$ is computed by placing a car every $6m$ at every road. It is assumed that every car represents the center of a Gaussian kernel, and it contributes to the total density within the radius set by the standard deviation of the Gaussian function. Here we assume that each vehicle has influence within $70m$ radius around its position. The Gaussian Kernel estimation is used to define densities everywhere in a continuum two-dimensional plane from vehicles' positions. Further, we assume that $\rho_{c,j} = \rho_{max,j}/3$ everywhere, which allows us also to calculate the negative kinematic wave speed ω_j and the roads' capacities $\phi_{max,j}$. Then, these parameters are translated into NSWE-formulation using the network geometry, see Section 4.2 for more details.

In order to determine the traffic flow direction, we use information on turning ratios α_{ij} for each road i towards road j that are calculated as

$$\alpha_{ij} = \frac{\phi_{max,j}}{\sum_{k=1}^{n_{out}} \phi_{max,k}}.$$

Then, supply coefficients β_{ij} are calculated using (7). Both ratios α and β are translated into NSWE-formulation as in (17) and (18). Further, we use the coordinates of roads' both ends to determine its length l_j and orientation angle θ_j , from which we then obtain L , $\overline{\cos \theta}$, $\overline{\sin \theta}$ in NSWE-formulation as described in Section 4.4.

Then, we approximate all these intersection and FD parameters for every cell (i, j) using Inverse Distance Weighting method as described in Section 4.5.

In general, low values of weighting parameter η from (29) imply that only the global trend of the density propagation is reproduced, while high values of η imply that the density follows more precisely the location of real roads (see [21] for more details). For the results presented in this section, we chose $\eta = 20$, which is a relatively low value.

We proceed as follows. First of all, we load the Grenoble network to Aimsun (see Fig.7b)), and let the cars enter the domain through its boundaries by specifying inflows. We choose inflow such that the main flow of cars comes from the South of the area. The microsimulations evolve for 2.5 minutes, and then the state is saved and later used as an initial condition for both Aimsun and numerical simulation of the NSWE-model. Afterwards, we continue the microsimulation on Aimsun until we do not perceive any structural changes in the state, which indicates that a steady state has been achieved. The results are saved as vehicles' positions at all time instants. Therefore, we use the density reconstruction procedure to be able to transform the standard Aimsun data into a density distribution (Gaussian Kernel estimation, see the details above and also [21]). The Gaussian Kernel estimation is also used to smooth inflows such that they enter the domain in a continuous line rather than at discrete points of space. Notice that we set constant inflows at network boundaries in order to let the system converge to a steady state, since steady states are easier to compare. We then perform a numerical simulation of the NSWE-model as described in the previous subsection using the initial conditions from Aimsun.

The results are depicted in Figure 8, where the comparison of both scenarios is shown for $t \in (0, 50)min$. We see that in both cases the distributions look quite similar but not identical, which might be caused by several things. In Aimsun, vehicles are restricted to move only on real physical roads, while more freedom of movement is perceived in a PDE-driven system. Moreover, in Aimsun, turning ratios indicate the probability with which a car turns to one or another road, whenever it reaches an intersection at some time instant. Thus, turning ratios in Aimsun should be understood as mathematical expectation rather than deterministic values. Hence, it often appears that scenarios

in Aimsun, having the same inputs, converge to different density distributions, since vehicles might get stuck in different parts of the city, while this is unlikely to happen during the numerical simulation of NSWE-model, where cars move on a continuum space. However, on a global scale traffic regimes seem to be reproduced correctly in most parts of the city.

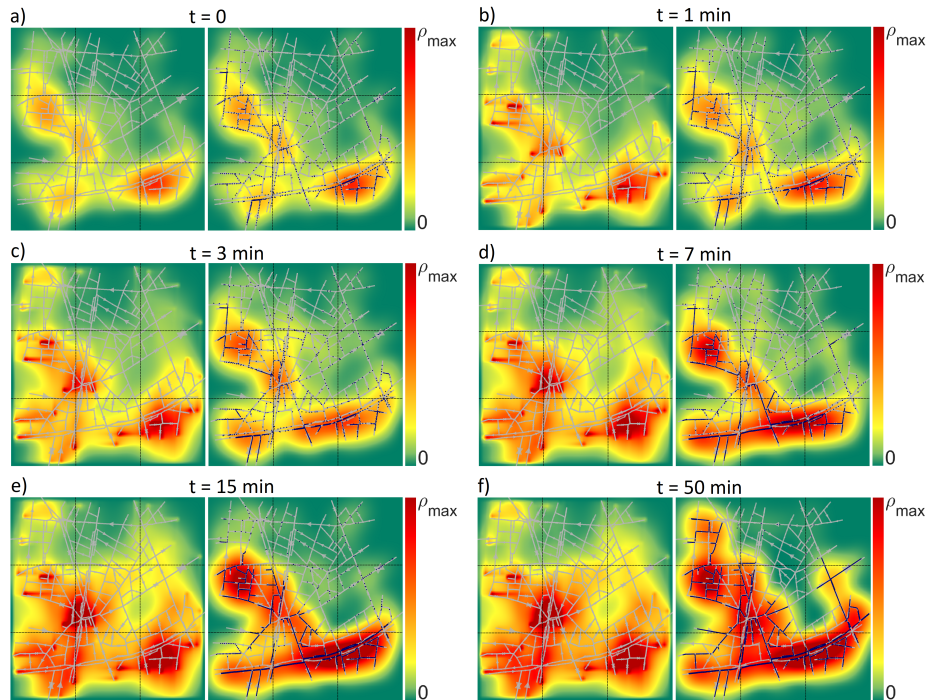


Figure 8: Congestion formation in Grenoble downtown for $t \in (0, 50)min$: numerical simulation of NSWE-model (left plots) and Aimsun (right plots) using weighting parameter $\eta = 20$. Blue dots denote vehicles' positions in Aimsun. Black dashed lines separate Grenoble in zones used for the calculation of SSIM index.

Let us now compute the structural similarity index defined in (36) to compare two density distributions from Fig.8. For that, let us divide our domain into 9 windows of equal size as drawn in Fig.9a). We do this in order to be able to compare density distributions zone-by-zone. The zones are numbered from top left to bottom right, as shown in Fig.9a). The SSIM index of the whole domain

is then calculated as the mean value \overline{SSIM} over all zones:

$$\overline{SSIM}(\bar{\rho}_1, \bar{\rho}_2) = \frac{\sum_{l=1}^{N_{zones}} SSIM_l \mu_l(\bar{\rho}_2)}{\sum_{l=1}^{N_{zones}} \mu_l(\bar{\rho}_2)}, \quad (38)$$

where $N_{zones} = 9$ is the total number of zones in the domain, $SSIM_l$ is referred to the SSIM index of zone l each given by (36), and $\mu_l(\bar{\rho}_2)$ is the corresponding weight of the zone based on its occupancy level in the reference distribution (here, $\bar{\rho}_2$ is the total density in Aimsun). Thus, the fewer cars a zone has, the smaller is its weight. The weights are assigned in order to avoid giving too much importance to zones that are currently almost empty. Notice that $\mu_l(\bar{\rho}_2(t))$ is a time-dependent parameter.

In its original formulation, the SSIM index varies from -1 to 1 . In order to facilitate the interpretation of the SSIM index in the context of density comparison, we make it range to be $SSIM \in [0, 1]$ by doing $(SSIM + 1)/2$. Thus, $SSIM = 1$ implies that two distributions are identical, and $SSIM = 0$ means that one distribution is completely the opposite of the second one (inverted image).

The SSIM index of corresponding zones in both distributions is depicted as a function of time in Fig.9b). It seems that the most problematic zones are the most empty ones that are concentrated in the upper part of the domain, while the best captured zones are 4 and 9, which are the most congested ones. This can be explained by the fact that the main vehicle flow enters the domain from the South (as prescribed by the boundary conditions in our scenario), where they build the most congested areas. Thus, cars might not have reached the upper part in Aimsun, since they got stuck in the Southern part of the area.

Finally, in order to enable a quantitative comparison of the density in the whole Grenoble area, the SSIM index is averaged over all zones by using (38), and we obtain the result depicted in Fig.10. Thereby, we can see that the overall SSIM index is approximately equal to 0.9 ($\approx 90\%$ accuracy), which indicates that the congested steady state is close to be reproduced correctly by our model

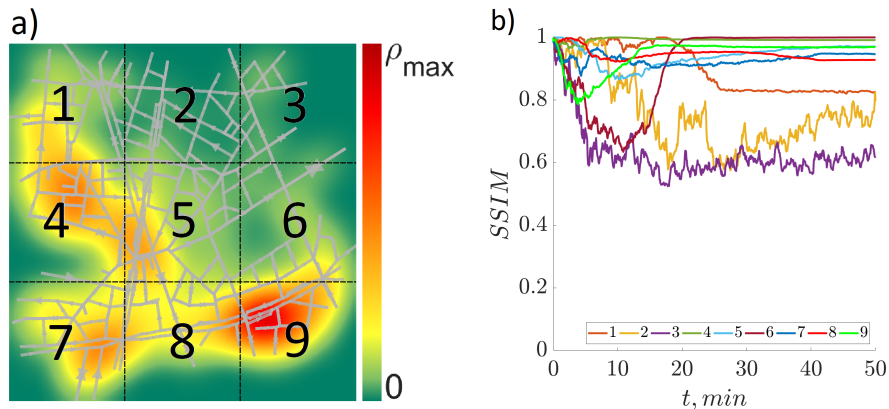


Figure 9: a) Zone numbering in Grenoble network; b) The SSIM index of each zone $SSIM_l$ with $l = \{1\dots 9\}$.

(28).

6.4. Model Validation using Real Data

For the model validation with real data, we make use of the Grenoble Traffic Lab for Urban Networks known as GTL Ville, see <http://gtlville.inrialpes.fr/>. This is an experimental platform for real-time collection of traffic data coming from a network of stationary flow sensors installed in Grenoble downtown, see Fig.11. This platform also provides real-time traffic indicators oriented towards the users of the city, traffic operators and researchers. The collected data and computed indicators are available for download at the GTL website.

The maximal densities at every road $\rho_{max,j}$, capacities $\phi_{max,j}$, road lengths l_j and orientations θ_j are the same as described above, since these parameters are defined by the network topology, which remains the same for the real-life experiment. However, the free-flow speed data are now taken from floating car data reported from several vehicles that are equipped with devices such as a GPS navigator. The free-flow speed is estimated as the maximal speed of a vehicle in the absence of other cars, and it starts decreasing as the density of surrounding cars increases. It is worth noting that, in general, the free-flow

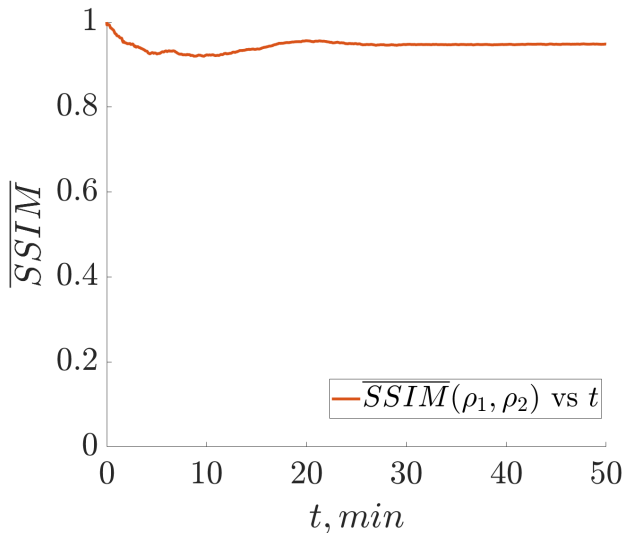


Figure 10: Mean value over zones of \overline{SSIM} computed by (38) between densities in Aimsun and in numerical simulation of NSWE as a function of time for weighting parameter $\eta = 20$.

speed is lower than the corresponding speed limit value, since in reality cars lose their velocity, e.g., by stopping at traffic lights.

Now let us explain how do we get turning ratios α_{ij} . These data are obtained from automatic vehicle identifiers using Bluetooth devices that were installed at adjacent incoming and outgoing roads of 12 intersections in total, see their location in Fig.11b). These identifiers are able to detect vehicles equipped with another Bluetooth device, which enables to assign the origin and destination road of individual vehicles. For the estimation of the remaining turning ratios (since there are more than 12 intersections in total), the information on road importance is used, and then the optimization problem minimizing the deviation of predicted and actual flows is solved.

Finally, we also get the estimated density values for every road ρ_j for every minute of the 8th of January 2021 from 6am to 9pm, as well as inflows and outflows at domain boundaries. Notice that in this scenario inflows are time-dependent functions. Estimation of free-flow speed, turning ratios and density reconstruction is described in more details in [33].

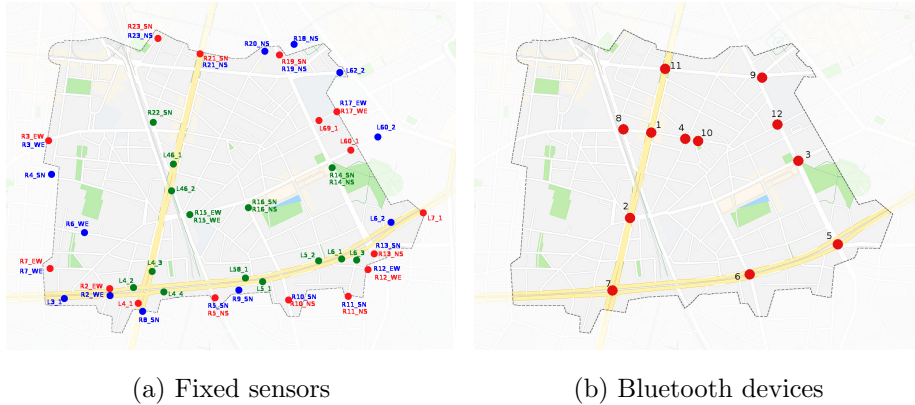


Figure 11: Sensor location in Grenoble downtown: (a) fixed flow sensors: R denote radars and L denote induction loops; (b) automatic vehicle identifiers using Bluetooth installed at 12 intersections of Grenoble during a measurement campaign lasting 1 week. These figures are taken from [32].

On Fig.11a) the sensors marked in blue are those giving boundary inflows and red sensors give boundary outflows. Sensors marked in green were used for the validation of state estimation procedure. Notice that state estimation procedure is not free of error and it does not reconstruct the state exactly, since there are only a limited number of sensors due to economical cost.

In order to get density values all over the continuum plane, i.e., at every point in Grenoble downtown (not only at physical roads), we divide each road into 10 parts, and at the boundary between each part we set a group of vehicles. We then assume that all these cars contribute to the global density around $70m$ from its positions using Gaussian Kernel Estimation. We also use Gaussian Kernel Estimation for the inflow values, as it was done in the previous example.

The results are depicted in Fig.12, where the comparison of two density distributions is shown. Again, we see that in both cases the distributions look quite similar. The first possible reason for these distributions to be non-identical is the probabilistic nature of turning ratios in reality opposed to deterministic nature in numerical simulation. Another reason is that the NSW model does not include traffic lights, as well as it is not able to capture accidents or the effect of pedestrians crossing a road.

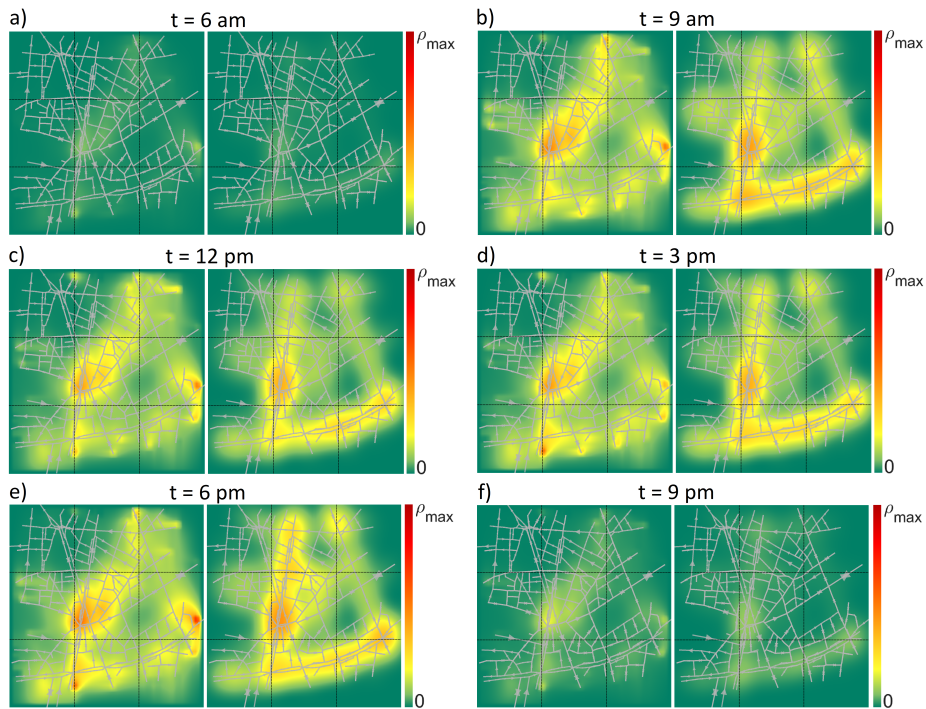


Figure 12: Dynamics of traffic density in Grenoble downtown from morning $t = 6am$ to evening $t = 9pm$: numerical simulation of NSWE-model (left plots) and real data (right plots). Weighting parameter $\eta = 20$.

Another source of mismatch could be induced by inflows and outflows data. The problem is that the data represent estimated measurements of the flows in the city that we can not enforce in our system, since there is always a demand-supply problem that needs to be solved, i.e.,

$$\phi^{source} = \min(D_{ext}, S(\rho)), \quad \phi^{sink} = \min(D(\rho), S_{ext}),$$

where ext is used in the subscript to highlight that these functions depend on what happens outside the domain. Thus, the data that we have are not related to demand and supply at domain boundaries but to actual inflow $\hat{\phi}^{source}$ and outflow $\hat{\phi}^{sink}$ of the system (we use hats to denote the measurement data).

To understand which problems can be provoked by these issues, let us consider some measured outflow $\hat{\phi}^{sink}$, which in turn is also just a result of solving

the minimum between demand and supply, i.e.,:

$$\hat{\phi}^{sink} = \min(D(\hat{\rho}), S_{ext}), \quad (39)$$

where demand $D(\hat{\rho})$ depends on the measured density, which might be something different than the one we get from the numerical simulation of NSW. E.

For the numerical simulation, the best thing we can do with the data about the measured outflow $\hat{\phi}^{sink}$ is to use it as a supply of the external area:

$$\phi^{sink} = \min(D(\rho), \hat{\phi}^{sink}). \quad (40)$$

However, it follows from (39) that $\hat{\phi}^{sink} \leq S_{ext}$, where the equality holds in case of congested traffic. If the traffic is not congested, then setting our external supply to be equal to measured outflow might lead to blocking the cars at domain exit instead of letting them come out.

We compare two distributions again by using the weighted SSIM index averaged over 9 zones as in the previous case using (38) and (36), and depict the result in Fig.13a), while Fig.13b) is referred to the SSIM index for each zone computed using (36). Notice that the zone numbering here is the same as in Fig.9a). The worst captured zones are 1 and 2 located on the upper part of the city, and the best results are achieved for zones 5, 4 and 8. A possible reason might be the fact that the cars get stuck at the bottom of the city in the real experiment, while they more freely in a PDE governed system. In general, notice that the best results are achieved for the time when the congestion level is the highest, as we can see from Fig. 13a). This is related to the weighting parameters used for calculation of SSIM (38). Weights tend to introduce more noisiness into computation, when there are only a few cars in the city. Finally, recall that the real-life data are also an approximation, since these densities are obtained by the estimation procedure that is not error-free due to the lack of sensors at every road. On average, the total SSIM index is around 0.75 (75% accuracy), which indicates that two density distributions are still quite close.

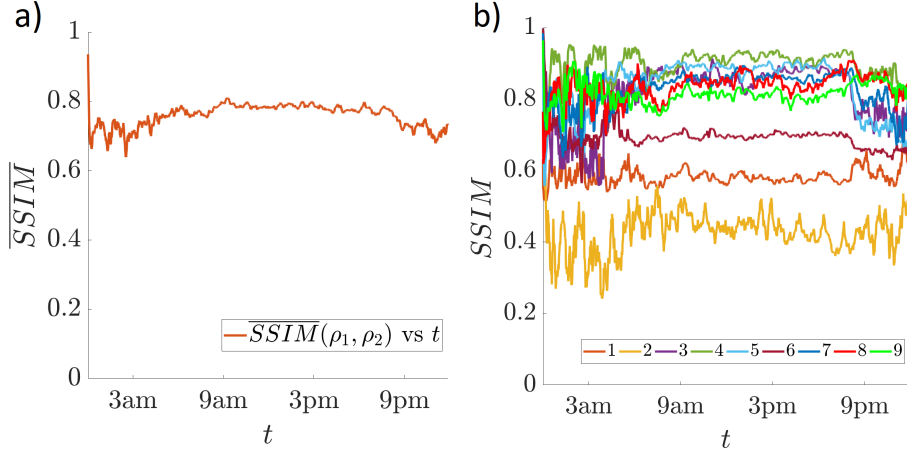


Figure 13: a) Mean value of \overline{SSIM} computed by (38) between the density ρ_1 predicted by numerical simulation of NSWE-model and the density ρ_2 estimated from real data as a function of time; b) The SSIM index of each zone $SSIM_l$ with $l = \{1 \dots 9\}$. Weighting parameter: $\eta = 20$.

6.5. Reproducibility of the results

It is worth noting that the source code used for model validation is an *open source* project that you can find here: <https://github.com/Lyurlik/multidirectional-traffic-model>. The README.md file contains all the essential information about the code structure and the data files such that anyone can get use of it for different purposes. Thus, the results are made to be reproducible.

This code is used to produce two different vehicle density distributions: the one predicted by numerical simulation of NSWE model (28), and the other density is the one reconstructed from data obtained from real sensors.

In order to run the code, you need to have the following files:

Network topology

1. `../ModelValidation/IntersectionTable.csv` – contains information about intersections: x and y coordinates of every intersection (columns 1 and 2), its ID (column 3) and whether it is a node on border (column 4), which means that this intersection is located at domain’s boundary through

which vehicles may enter (inflows), or exit (outflows);

2. *"../ModelValidation/RoadTable.csv"* – contains information about roads: ID1 and ID2 (columns 3 and 4) are the id's of corresponding intersections that the road is connecting, ID_road (column 5) is the road's ID, max_vel (column 6) is its free-flow limit estimated from real measurements, then we have number of lanes (column 7) and road's length (column 8);
3. *"../ModelValidation/TurnTable.csv"* – contains turning ratios between any pair of roads: ID1 of incoming road (column 1), ID2 of outgoing road (column 2) and the turning ratio between these roads (column 5).

Data from real sensors

5. *"../ModelValidation/Timestamp.csv"* – contains time in seconds at which the data are given (unix timestamp), the time step equals to one minute;
6. *"../ModelValidation/Density.csv"* – contains estimated density from real sensors: first number is road_id followed by its density (that is assumed to be constant within one road) at all time instants, then the next road_id with its density data for each time instant and so on;
7. *"../ModelValidation/AllInflows.csv"* – contains inflow values (in veh/hour) for every road for every time step (one minute). If road is outgoing from intersection that is not on border, then the inflow value is zero;
8. *"../ModelValidation/AllOutflows.csv"* – contains outflow values (in veh/hour) for every road for every time step (one minute). If road is incoming into intersection that is not on border, then the outflow value is zero.

Code structure

The main file of the project is **mainwindow.cpp**: in its constructor we specify the file names to be loaded, start simulation starting time (line 26) and simulation step size (line 28). The paths to files containing network and density data are also specified here. We can also change there the weighting parameter η used to approximate parameters for every cell (line 4), and parameter d_0 (line 5) is used for Gaussian Kernel estimation.

Other important classes are:

- **UrbanNetwork**, which contains all the network geometry information (this is where all the network files are read). This network is used for both densities. In its function *loadRoads*, one needs to specify the minimum distance between the heads of two consequential vehicles.
- **NSWEmodel**, which contains translation procedure of all network and intersection parameters into NSWE-formulation (function *processIntersections*). After all parameters are defined in NSWE, it calls *constructInterpolation* function that approximates these parameters defined for every intersection to be defined on every cell of a network. Then update is performed, where the Godunov numerical scheme is applied for the state update using NSWE model. There is also a function *getSSIMdiff_mean_weighted* used to compute the weighted SSIM index between two densities (38).
- **GrenobleData**, where all the data estimated from the real-life experiments are loaded. In function *reconstructDensity* the density initially given for each road is defined for every cell. Thereby, every road is divided in 10 parts and density values are presented as points on the border between these parts. Then Gaussian Kernel estimation is used to determine density for every cell in the domain.
- **TrafficSystem**, which implements concurrent thread for parallel NSWE simulation relative to the main visualization thread.

7. Conclusions

To summarize, we have derived a macroscopic continuous traffic flow model that can be used for modelling on large-scale networks. The derivation was done analytically, using only a few assumptions on networks: they must be well-designed in terms of maximal flows, and each outgoing road possesses some particular supply for the flow from incoming roads. The model has been analysed, and it was shown to be hyperbolic, which is a desirable property signif-

icantly simplifying the analysis for future tasks such as explicit control design or steady-state estimation. The model predicts evolution of traffic in four cardinal directions. The propagation of traffic flow in each direction is driven by the demand-supply concept that uses a fundamental diagram whose parameters are determined by the network topology, as well as by the data from real-life experiments. Moreover, vehicles moving in some layer can switch to another layer, which means that there exists mixing between different layers, which is an important aspect to be included into the model due to its physical ubiquity. The model prediction results have been validated using experimental platform GTL Ville that provides real-time data from a network of real sensors installed in Grenoble. We have made this project to be an open source such that the results are reproducible and could be used for future studies.

As a promising direction for the future development of optimally operating transportation systems, it would be interesting to use this model to solve traffic control tasks on urban networks such as vehicle density stabilization around some desired equilibrium value, e.g., throughput maximization.

Appendix A. List of notations

Appendix A.1. Road formulation

Variable	Meaning	Units
$\rho(x, y, t)$	vehicle density	veh/m
$\Phi(x, y, \rho)$	flow function	veh/s
$v(x, y)$	kinematic wave speed in free-flow regime	m/s
$\omega(x, y)$	kinematic wave speed in congested regime	m/s
$\rho_c(x, y)$	critical vehicle density	veh/m
$\phi_{max}(x, y)$	flow capacity	veh/s
$D(\rho)$	demand function	veh/s
$S(\rho)$	supply function	veh/s
ϕ_i^{in}	inflow to intersection from road i	veh/s
ϕ_j^{out}	outflow from intersection to road j	veh/s
ψ_j^{in}	inflow into road j	veh/s
ψ_j^{out}	outflow from road j	veh/s
n_{in}	number of incoming roads for intersection	-
n_{out}	number of outgoing roads from intersection	-
ϕ_{ij}	flow from road i to road j	veh/s
α_{ij}	turning ratio from road i to road j	-
β_{ij}	supply coefficient of road j for the flow from road i	-
D_{ij}	flow demand of road i to enter road j	veh/s
S_{ij}	supply of road j for flow coming from road i	veh/s
θ_i	angle that road i builds with East	degrees
l_i	length of road i	m

Appendix A.2. NSWE formulation

Variable	Meaning	Units
$p_\theta^N, p_\theta^S, p_\theta^W, p_\theta^E$	projection coefficients wrt corresponding directions	-
$P_{in} \in \mathbb{R}^{4 \times n_{in}}$	projection matrix for incoming roads into NSWE	-
$P_{out} \in \mathbb{R}^{4 \times n_{out}}$	projection matrix for outgoing roads into NSWE	-
$\bar{\rho}(x, y, t)$	4-dim density vector	veh/m
$\bar{\Phi}(x, y, \bar{\rho})$	4-dim flow function	veh/s
$\bar{\rho}_{max}(x, y)$	4-dim maximal density	veh/m
$\bar{v}(x, y), \bar{\omega}(x, y)$	4-dim kinematic wave speeds	m/s
$\bar{\rho}_c(x, y)$	4-dim critical density	veh/m
$\bar{\phi}_{max}(x, y)$	4-dim flow capacity	veh/s
$\bar{D}(x, y, \bar{\rho})$	4-dim demand function	veh/s
$\bar{S}(x, y, \bar{\rho})$	4-dim supply function	veh/s
$\bar{\phi}_N^{in}(x, y)$	inflow into intersection in the North direction	veh/s
$\bar{\phi}_N^{out}(x, y)$	outflow from intersection in the North direction	veh/s
$\bar{\phi}_{NE}(x, y)$	partial flow from North to East wrt intersection	veh/s
$\bar{\psi}_N^{in}(x, y)$	inflow into outgoing road in the North direction	veh/s
$\bar{\psi}_N^{out}(x, y)$	outflow from outgoing road in the North direction	veh/s
$\bar{\psi}_{NE}(x, y)$	partial flow from North to East wrt outgoing roads	veh/s
$\bar{\alpha}_{EN}(x, y)$	turning ratio from East to North layer	-
$\bar{\beta}_{EN}(x, y)$	supply of East layer for the flow from the North	-
$\overline{\cos \theta}(x, y),$ $\overline{\sin \theta}(x, y)$	average direction parameters of intersection	-
$L(x, y)$	average length of outgoing roads of intersection	m

Appendix B. Proof that $\bar{\psi}_N = \min(\bar{D}_N, \bar{S}_N)$

Here we prove that the flow in some direction (here North) can be written as a function of demand and supply of the same direction:

$$\bar{\psi}_N = \min(\bar{D}_N, \bar{S}_N),$$

which allows to simplify the model (24).

Let us consider $(1 - \gamma)\bar{\psi}_{EN} + \gamma\bar{\psi}_{NE}$ from (25). By definition (16) we get:

$$\bar{\psi}_{EN} = \min(\bar{\alpha}_{EN}\bar{D}_E, \bar{\beta}_{EN}\bar{S}_N), \quad \bar{\psi}_{NE} = \min(\bar{\alpha}_{NE}\bar{D}_N, \bar{\beta}_{NE}\bar{S}_E).$$

Notice that now we omit indices "in" and "out" in the demand and supply functions, since they are now referred to the same point. This comes from the continuation, due to which intersections are now assumed to be infinitesimally small in space.

Recall that by definition of the demand-supply formulation, if $\bar{D}_E < \bar{\psi}_{max,E}$, then $\bar{S}_E = \bar{\psi}_{max,E}$ and vice versa. The same holds for \bar{D}_N and \bar{S}_N . For simplicity of writing denote $Q(\gamma) = (1 - \gamma)\bar{\psi}_{EN} + \gamma\bar{\psi}_{NE}$. We will prove that there always exists γ such that $Q(\gamma) = \min(\bar{\alpha}_{NE}\bar{D}_N, \bar{\beta}_{EN}\bar{S}_N)$. There are no more than six different possibilities:

1. $\bar{\alpha}_{EN}\bar{D}_E < \bar{\beta}_{EN}\bar{S}_N$ and $\bar{\alpha}_{NE}\bar{D}_N > \bar{\beta}_{NE}\bar{S}_E$. From the first inequality we obtain

$$\bar{\alpha}_{EN}\bar{D}_E < \bar{\beta}_{EN}\bar{S}_N \leq \bar{\beta}_{EN}\bar{\psi}_{max,N} = \bar{\alpha}_{EN}\bar{\psi}_{max,E},$$

where the last equality comes for the assumption that the network is well-designed (27). Thus, we get that

$$\bar{D}_E < \bar{\psi}_{max,E}.$$

From the other side, if we consider the second inequality, we get

$$\bar{\beta}_{NE}\bar{S}_E < \bar{\alpha}_{NE}\bar{D}_N \leq \bar{\alpha}_{NE}\bar{\psi}_{max,E} \Rightarrow \bar{S}_E < \bar{\psi}_{max,E}.$$

According to the demand-supply formulation, it is however not possible that $\bar{D}_E < \bar{\psi}_{max,E}$ and $\bar{S}_E < \bar{\psi}_{max,E}$ hold at the same time. Thus, this case can be excluded from consideration.

2. $\bar{\alpha}_{EN}\bar{D}_E > \bar{\beta}_{EN}\bar{S}_N$ and $\bar{\alpha}_{NE}\bar{D}_N < \bar{\beta}_{NE}\bar{S}_E$. This case is also impossible, since from the first inequality we get $\bar{S}_N < \bar{\psi}_{max,N}$ and from the second inequality we get $\bar{D}_N < \bar{\psi}_{max,N}$, which violates the demand-supply formulation.

3. $\bar{\alpha}_{NE}\bar{D}_N \leq \bar{\beta}_{NE}\bar{S}_E$ and $\bar{\alpha}_{NE}\bar{D}_N \leq \bar{\beta}_{EN}\bar{S}_N$. In this case taking $\gamma = 1$ results into

$$Q(1) = \bar{\psi}_{NE} = \min(\bar{\alpha}_{NE}\bar{D}_N, \bar{\beta}_{NE}\bar{S}_E) = \bar{\alpha}_{NE}\bar{D}_N,$$

which in combination with the second inequality yields

$$Q(1) = \min(\bar{\alpha}_{NE}\bar{D}_N, \bar{\beta}_{EN}\bar{S}_N),$$

which is the desired property achieved with $\gamma = 1$.

4. $\bar{\alpha}_{EN}\bar{D}_E \leq \bar{\beta}_{EN}\bar{S}_N$, $\bar{\alpha}_{NE}\bar{D}_N \leq \bar{\beta}_{NE}\bar{S}_E$ and $\bar{\alpha}_{NE}\bar{D}_N > \bar{\beta}_{EN}\bar{S}_N$.

By the first inequality for $\gamma = 0$ we obtain the following:

$$\begin{aligned} Q(0) &= \bar{\psi}_{EN} = \min(\bar{\alpha}_{EN}\bar{D}_E, \bar{\beta}_{EN}\bar{S}_N) \\ &= \bar{\alpha}_{EN}\bar{D}_E \leq \bar{\beta}_{EN}\bar{S}_N. \end{aligned}$$

By the second inequality for $\gamma = 1$ we obtain

$$Q(1) = \bar{\psi}_{NE} = \min(\bar{\alpha}_{NE}\bar{D}_N, \bar{\beta}_{NE}\bar{S}_E) = \bar{\alpha}_{NE}\bar{D}_N,$$

and from the third inequality we get

$$Q(1) > \bar{\beta}_{EN}\bar{S}_N.$$

Combining these results all together, we show the desired property:

$$\begin{cases} Q(0) \leq \bar{\beta}_{EN}\bar{S}_N, & \Rightarrow \exists \gamma \in [0, 1) : Q(\gamma) = \bar{\beta}_{EN}\bar{S}_N = \\ Q(1) > \bar{\beta}_{EN}\bar{S}_N, & \min(\bar{\alpha}_{NE}\bar{D}_N, \bar{\beta}_{EN}\bar{S}_N). \end{cases}$$

5. $\bar{\alpha}_{EN}\bar{D}_E \leq \bar{\beta}_{EN}\bar{S}_N$, $\bar{\alpha}_{NE}\bar{D}_N \leq \bar{\beta}_{NE}\bar{S}_E$ and $\bar{\alpha}_{NE}\bar{D}_N \leq \bar{\beta}_{EN}\bar{S}_N$. The analysis here is the same as in case (3): we take $\gamma = 1$, which results in $Q(1) = \min(\bar{\alpha}_{NE}\bar{D}_N, \bar{\beta}_{NE}\bar{S}_E)$.

6. $\bar{\alpha}_{EN}\bar{D}_E \geq \bar{\beta}_{EN}\bar{S}_N$, $\bar{\alpha}_{NE}\bar{D}_N \geq \bar{\beta}_{NE}\bar{S}_E$ and $\bar{\alpha}_{NE}\bar{D}_N > \bar{\beta}_{EN}\bar{S}_N$. Here we also proceed as in case (4): taking $\gamma = 0$ results in $Q(0) = \bar{\beta}_{EN}\bar{S}_N$. Further, by the second condition $Q(1) \leq \bar{\alpha}_{NE}\bar{D}_N$, therefore there exists $\gamma \in [0, 1]$ such that $Q(\gamma) = \min(\bar{\alpha}_{NE}\bar{D}_N, \bar{\beta}_{EN}\bar{S}_N)$.

Therefore, if we assume that we can manipulate gamma independently for every pairwise flow, we can summarize the discussion above in the following formula: $(1 - \gamma)\bar{\psi}_{EN} + \gamma\bar{\psi}_{NE} = \min(\bar{\alpha}_{NE}\bar{D}_N, \bar{\beta}_{EN}\bar{S}_N)$. This leads to the following transformation of (25):

$$\begin{aligned} \bar{\psi}_N &= \bar{\psi}_{NN} + \min(\bar{\alpha}_{NS}\bar{D}_N, \bar{\beta}_{SN}\bar{S}_N) + \\ &+ \min(\bar{\alpha}_{NW}\bar{D}_N, \bar{\beta}_{WN}\bar{S}_N) + \min(\bar{\alpha}_{NE}\bar{D}_N, \bar{\beta}_{EN}\bar{S}_N). \end{aligned}$$

Finally, using once again the approximation, where we replace the sum of minima with the minimum of sums, we can write

$$\begin{aligned} \bar{\psi}_N &= \min(\bar{\alpha}_{NN}\bar{D}_N + \bar{\alpha}_{NS}\bar{D}_N + \bar{\alpha}_{NW}\bar{D}_N + \bar{\alpha}_{NE}\bar{D}_N, \\ &\bar{\beta}_{NN}\bar{S}_N + \bar{\beta}_{SN}\bar{S}_N + \bar{\beta}_{WN}\bar{S}_N + \bar{\beta}_{EN}\bar{S}_N) = \min(\bar{D}_N, \bar{S}_N), \end{aligned}$$

which is exactly the property we wanted to prove (26).

Acknowledgment

The Scale-FreeBack project has received funding from the European Research Council (ERC) under the European Unions Horizon 2020 research and innovation programme (grant agreement N 694209).

References

- [1] J. M. Lighthill, G. Whitham, On kinematic waves, ii: A theory of traffic flow on long crowded roads, Proc. R. Soc. Lond. A 229 (1955) 317–345. doi:10.1098/rspa.1955.0089.
- [2] P. Richards, Shock waves on the highway, Operations Research 47 (1) (1956) 42–51. doi:10.1287/opre.4.1.42.
- [3] C. F. Daganzo, The cell transmission model: A dynamic representation of highway traffic consistent with the hydrodynamic theory, Transportation Research Part B: Methodological 28 (4) (1994) 269–287. doi:10.1016/0191-2615(94)90002-7.

- [4] H. Holden, N. H. Risebro, A mathematical model of traffic flow on a network of unidirectional roads, *SIAM J. Math. Anal.* 26 (4) (1995) 999–1017. doi:10.1137/S0036141093243289.
- [5] G. M. Coclite, M. Garavello, B. Piccoli, Traffic flow on a road network, *SIAM J. Math. Anal.* 36 (6) (2005) 1862–1886. doi:10.1137/S0036141004402683.
- [6] C. F. Daganzo, The cell transmission model, part ii: network traffic, *Transportation Research Part B: Methodological* 29 (2) (1995) 79–93. doi:10.1016/0191-2615(94)00022-R.
- [7] M. Garavello, B. Piccoli, *Traffic Flow on Networks. Conservation Laws Models*, AIMS Series on Applied Mathematics, Springfield, MO, USA, 2006.
- [8] R. J. Smeed, The road capacity of city centers, *Traffic Engineering and Control* 8 (1966) 455–458.
- [9] J. M. Thomson, Speeds and flows of traffic in central london: 2. speed-flow relations, *Traffic Engineering and Control* 8 (1967) 721–725.
- [10] R. Herman, I. Prigogine, A two-fluid approach to town traffic, *Science* 204 (1979) 148–151. doi:10.1126/science.204.4389.148.
- [11] H. W. Ho, S. C. Wong, Two-dimensional continuum modeling approach to transportation problems, *Journal of Transportation Systems Engineering and Information Technology* 6 (6) (2006) 53 – 68. doi:10.1016/S1570-6672(07)60002-6.
- [12] N. Geroliminis, C. F. Daganzo, Existence of urban-scale macroscopic fundamental diagrams: Some experimental findings, *Transportation Research Part B: Methodological* 42 (2008) 756–770. doi:10.1016/j.trb.2008.02.002.

- [13] C. F. Daganzo, N. Geroliminis, An analytical approximation for the macroscopic fundamental diagram of urban traffic, *Transportation Research Part B: Methodological* 42 (2008) 771–781. doi:10.1016/j.trb.2008.06.008.
- [14] M. Hajiahmadi, V. L. Knoop, B. De Schutter, H. Hellendoorn, Optimal dynamic route guidance: A model predictive approach using the macroscopic fundamental diagram, in: *16th International IEEE Conference on Intelligent Transportation Systems (ITSC 2013)*, 2013, pp. 1022–1028. doi:10.1109/ITSC.2013.6728366.
- [15] L. Leclercq, C. Parzani, V. L. Knoop, J. Amourette, S. P. Hoogendoorn, Macroscopic traffic dynamics with heterogeneous route patterns, *Transportation Research Part C: Emerging Technologies* 59 (2015) 292–307. doi:10.1016/j.trc.2015.05.006.
- [16] L. Tumash, C. Canudas-de-Wit, M. L. Delle Monache, Equilibrium manifolds in 2d fluid traffic models, in: *21th IFAC World Congress*, Berlin, Germany, July 2020. doi:hal-02513273v2f.
- [17] R. Aghamohammadi, J. A. Laval, Dynamic traffic assignment using the macroscopic fundamental diagram: A review of vehicular and pedestrian flow models, *Transportation Research Part B: Methodological* 137 (2020) 99–118. doi:10.1016/j.trb.2018.10.017.
- [18] R. L. Hughes, A continuum theory for the flow of pedestrians, *Transportation Research Part B: Methodological* 36 (6) (2002) 507–535. doi:10.1016/S0191-2615(01)00015-7.
- [19] Y. Jiang, S. Wong, H. Ho, P. Zhang, R. Liu, A. Sumalee, A dynamic traffic assignment model for a continuum transportation system, *Transportation Research Part B: Methodological* 45 (2) (2011) 343–363. doi:10.1016/j.trb.2010.07.003.
- [20] J. Du, S. Wong, C.-W. Shu, T. Xiong, M. Zhang, K. Choi, Revisiting jiang’s

- dynamic continuum model for urban cities, *Transportation Research Part B: Methodological* 56 (2013) 96–119. doi:10.1016/j.trb.2013.07.001.
- [21] S. Mollier, M. L. Delle Monache, C. C. de Wit, B. Seibold, Two-dimensional macroscopic model for large scale traffic networks, *Transportation Research Part B: Methodological* 122 (2019) 309 – 326. doi:10.1016/j.trb.2019.02.016.
- [22] Z. Y. Lin, S. C. Wong, P. Zhang, Y. Q. Jiang, K. Choi, Y. C. Du, A predictive continuum dynamic user-optimal model for a polycentric urban city, *Transportmetrica B: Transport Dynamics* 5 (3) (2017) 228–247. doi:10.1080/21680566.2016.1163297.
- [23] S. Mollier, M. L. Delle Monache, C. Canudas-de-Wit, A step towards a multidirectional 2d model for large scale traffic networks, in: *TRB 2019 - 98th Annual Meeting Transportation Research Board*, Washington D.C., USA, Jan. 2019, pp. 1–7. doi:hal-01948466.
- [24] R. Aghamohammadi, J. A. Laval, A continuum model for cities based on the macroscopic fundamental diagram: a semi-lagrangian solution method, *Transportation Research Procedia* 38 (2019) 380–400. doi:10.1016/j.trpro.2019.05.021.
- [25] D. Nikitin, C. C. de Wit, P. Frasca, A continuation method for large-scale modeling and control: from odes to pde, a round trip, arXiv:2101.10060.
- [26] B. D. Greenshields, J. R. Bibbins, W. S. Channing, H. H. Miller, A study of traffic capacity, *Highway Research Board proceedings* 1935.
- [27] D. Serre, *Systems of Conservation Laws I: Hyperbolicities, Entropies, Shock Waves*, Cambridge University Press, Cambridge, 1999.
- [28] R. Courant, K. Friedrichs, H. Lewy, On the partial difference equations of mathematical physics, *IBM Journal of Research and Development* 11 (2) (1967) 215–234. doi:10.1147/rd.112.0215.

- [29] S. K. Godunov, A difference method for numerical calculation of discontinuous solutions of the equations of hydrodynamics, *Matematicheskii Sbornik* 47 (3) (1959) 271–306.
- [30] R. Courant, E. Isaacson, M. Rees, On the solution of nonlinear hyperbolic differential equations by finite differences, *Communications on Pure and Applied Math.* 5 (1952) 243–255. doi:10.1002/cpa.3160050303.
- [31] Zhou Wang, A. C. Bovik, H. R. Sheikh, E. P. Simoncelli, Image quality assessment: from error visibility to structural similarity, *IEEE Transactions on Image Processing* 13 (4) (June 2004) 600–612. doi:10.1109/TIP.2003.819861.
- [32] M. Rodriguez-Vega, Optimal sensor placement and density estimation in large-scale traffic networks, PhD Thesis, University Grenoble Alpes, 2021.
- [33] M. Rodriguez-Vega, C. Canudas-de-Wit, H. Fourati, Urban network traffic state estimation using a data-based approach, in: *CTS 2021 - 16th IFAC Symposium on Control in Transportation Systems*, Lille, France, June 2021. doi:hal-03171255.